Journal of Medicinal Chemistry

ARTICLE

pubs.acs.org/jmc

Development of a Liver-Targeted Stearoyl-CoA Desaturase (SCD) Inhibitor (MK-8245) to Establish a Therapeutic Window for the Treatment of Diabetes and Dyslipidemia

Renata M. Oballa,*[,†] Liette Belair,[†] W. Cameron Black,[†] Kelly Bleasby,[‡] Chi Chung Chan,[†] Carole Desroches,[†] Xiaobing Du,[‡] Robert Gordon,[†] Jocelyne Guay,[†] Sebastien Guiral,[†] Michael J. Hafey,[‡] Emelie Hamelin,[†] Zheng Huang,[†] Brian Kennedy,[†] Nicolas Lachance,[†] France Landry,[†] Chun Sing Li,[†] Joseph Mancini,[†] Denis Normandin,[†] Alessandro Pocai,[‡] David A. Powell,[†] Yeeman K. Ramtohul,[†] Kathryn Skorey,[†] Dan Sørensen,[†] Wayne Sturkenboom,[†] Angela Styhler,[†] Deena M. Waddleton,[†] Hao Wang,[†] Simon Wong,[†] Lijing Xu,[†] and Lei Zhang[†]

[†]Merck Frosst Centre for Therapeutic Research, 16711 TransCanada Highway, Kirkland, Québec H9H 3L1, Canada

[‡]MerckResearch Laboratories, 126 East Lincoln Avenue, Rahway, New Jersey 07065-0900, United States

Supporting Information

ABSTRACT: The potential use of SCD inhibitors for the chronic treatment of diabetes and dyslipidemia has been limited by preclinical adverse events associated with inhibition of SCD in skin and eye tissues. To establish a therapeutic window, we embarked on designing liver-targeted SCD inhibitors by utilizing molecular recognition by liver-specific organic anion transporting polypeptides (OATPs). In doing so, we set out to target the SCD inhibitor to the organ believed to be responsible for the therapeutic efficacy (liver) while minimizing its exposure in the tissues associated with mechanism-based SCD depletion of essential lubricating lipids (skin and eye). These efforts led to the discovery of MK-8245 (7), a potent, liver-targeted SCD inhibitor with preclinical antidiabetic and antidyslipidemic efficacy with a significantly improved therapeutic window.

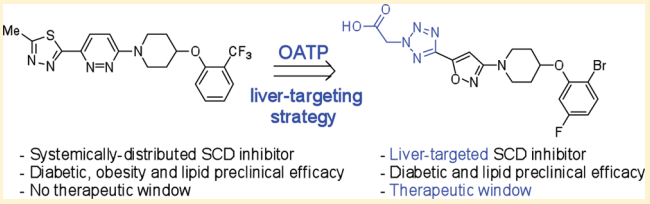

INTRODUCTION

One of the fundamental goals for pharmaceutical intervention is to achieve the desired efficacy with as few side effects as possible. This can be particularly challenging in cases where the target enzyme or receptor is ubiquitously expressed and deemed essential for certain physiological processes. One such target is stearoyl-CoA desaturase-1 (SCD1). SCD1 is the key enzyme involved in the synthesis of monounsaturated fatty acids and catalyzes the installation of a *cis*-double bond at the Δ9 position of long chain saturated fatty acyl-coenzyme A esters.[1] The monounsaturated lipid products (palmitoleoyl-CoA (C16:1) and oleoyl-CoA (C18:1)) are key building blocks in the synthesis of membrane phospholipids, cholesterol esters, and triglycerides. It has been reported that rodents deficient in SCD1 either by gene deletion,[2−4] antisense oligonucleotide (ASO) treatment,[5−7] or pharmacological inhibition[8−12] are resistant to diet-induced weight gain and have an improved insulin sensitivity, glucose tolerance, and lipid profile. In humans, elevated SCD1 levels are positively correlated with higher plasma triglycerides[13] as well as increased BMI and high insulin levels.[14] On the basis of the human and rodent findings, SCD1 represents an attractive novel therapeutic target for the treatment of type II diabetes, dyslipidemia, obesity, and metabolic diseases. However, in addition to the positive metabolic effects associated with SCD1 inhibition, there are reports of skin and eye abnormalities in the *SCD1*$^{-/-}$ mice[3,15] as well as in rodents treated with SCD1 inhibitors.[8−10] These adverse events (AEs) consist of dry eye, squinting, and alopecia and are believed to be due to mechanism-based depletion of essential SCD-derived lubricating lipids. Thus, the main challenge with developing a small molecule SCD inhibitor is to achieve adequate therapeutic efficacy without affecting the human skin and eye functions. Given the nonlife threatening nature of metabolic diseases, it is crucial to establish a sufficient therapeutic window for SCD inhibitors for treating metabolic syndromes before embarking on human clinical trials. One potential way to achieve a therapeutic window for SCD inhibition is to target the SCD inhibitor to the organ believed to be responsible for the therapeutic efficacy (liver) while minimizing its exposure in the tissues associated with mechanism-based SCD depletion of essential lubricating lipids (skin and eye).

Two pivotal SCD1 knockdown experiments provided evidence that it may be possible to develop a safe and effective SCD inhibitor for therapeutic application. First, treatment of mice with an SCD1 ASO resulted in ∼60−70% reduction of SCD1 mRNA in liver and fat and prevented diet-induced obesity and improved

Received: March 19, 2011
Published: June 10, 2011

Scheme 1. Synthesis of Tetrazole 4[a]

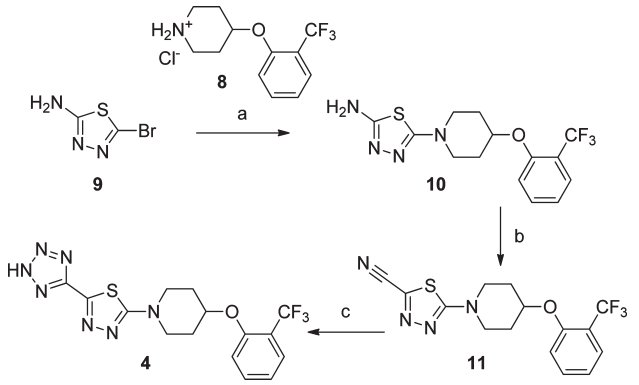

[a] Reagents and conditions: (a) **8**, K_2CO_3, DMF, 80 °C; (b) CuCN, *t*-BuONO, CH_3CN, 50−60 °C; (c) NaN_3, NMP, 130 °C.

insulin sensitivity.[5] Importantly, after 10 weeks of treatment with the SCD1 ASO, the mice did not demonstrate the hair, skin, and eye abnormalities observed either with SCD1 inhibitor-treatment or in the global *SCD1*$^{-/-}$ mice. Second, Cre-lox technology was used to generate mice with a liver-specific knockout of SCD1 (LKO),[4] and these mice were protected from high-carbohydrate diet-induced adiposity and hepatic steatosis. Unlike the global *SCD1*$^{-/-}$ mice showing alopecia and closed eyes, the LKO mice were indistinguishable from both wild-type and Lox mice (18 weeks).

In drug discovery, tissue-targeting refers to a process which delivers a pharmaceutical agent (small molecule or biologic) to the desired specific tissue. Targeting a pharmaceutical agent to the liver (i.e., liver-targeting) can be highly effective to treat liver-related diseases when it is essential to minimize exposure to other tissues where adverse events can occur as a result of mechanism-based or off target drug activity. To target a pharmaceutical agent to the liver, the following approaches have been studied: (i) nanoparticles to deliver incorporated therapeutic materials such as small molecules, proteins, genes, and siRNAs,[16] (ii) HepDirect cytochrome P450-activated prodrugs of certain small molecules such as nucleotides,[17] and (iii) utilization of liver-specific transport proteins.[18] The approach to liver-targeting outlined in this paper relies on the latter strategy. Described herein will be the strategy used to design liver-targeting SCD inhibitors and how this approach resulted in the discovery of the lead compound MK-8245 (**7**), which maintains preclinical pharmacological efficacy while significantly improving the therapeutic window compared to systemically distributed SCD inhibitors (i.e., **1**).

CHEMISTRY

The synthesis of the thiadiazole tetrazole **4** was prepared as described in Scheme 1. Starting with the bromo thiadiazole amine **9**, addition of the piperadine **8** under basic conditions resulted in the formation of the amine **10**. The amine **10** was then converted to the nitrile **11** using standard conditions and, finally, the tetrazole **4** was generated by reacting nitrile **11** with sodium azide. The syntheses of tetrazole **5** and the tetrazole acetic acid **6** are described in Scheme 2. The bromo thiadiazole **12** was reacted under basic conditions with the piperadine **13** to generate the nitrile **14**. Compound **5** was prepared by reacting nitrile **14** with sodium azide. Subsequent reaction of the tetrazole **5** with sodium

Scheme 2. Syntheses of Tetrazole 5 and Tetrazole Acetic Acid 6[a]

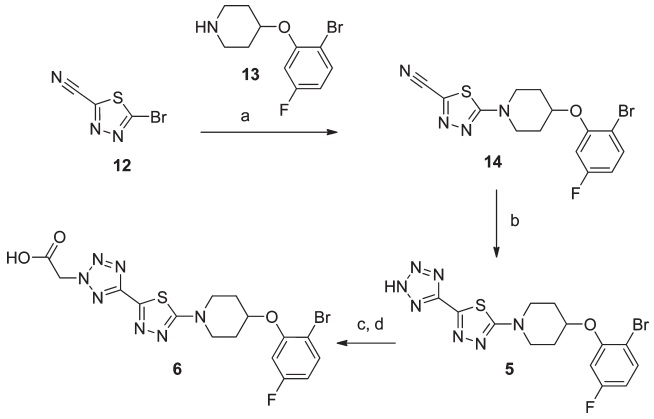

[a] Reagents and conditions: (a) **13**, iPr_2EtN, 1,4-dioxane; (b) NaN_3, NMP, 130 °C; (c) NaH, ethyl bromoacetate, DMF, −78 °C to rt; (d) NaOH, THF/MeOH.

hydride and ethyl bromoacetate generated two alkylated products, the major one bearing the ethylacetate at the N-2 position of the tetrazole. Upon chromatographic separation of the two alkylated products, the desired major product was subjected to basic ester hydrolysis to generate the desired tetrazole acetic acid **6**. The synthesis of the optimal liver-targeted tetrazole acetic acid **7** was prepared as outlined in Scheme 3. The key transformation is an unprecedented three-component 1,3-dipolar cycloaddition and nucleophilic substitution reaction between **13**, **15**, and **16** to give the isoxazole intermediate **17** in ∼20% yield. The mechanism of this transformation is still not clear. Because 3-bromoisoxazole is quite resistant to nucleophilic substitution, it is reasonable to hypothesize that the piperidine **13** and the dipole precursor **16** may react prior to the cycloaddition reaction with propiolate **15**. The ester group in compound **17**[19] was converted to the corresponding amide **18** by reaction with ammonium hydroxide. The amide **18** was then dehydrated to the nitrile **19** by reaction with trifluoroacetic anhydride. The nitrile **19** was converted to the tetrazole **20** and finally to the desired tetrazole acetic acid **7** in a similar manner as previously described for compound **6**.

RESULTS AND DISCUSSION

Strategy to Design a Liver-Targeted SCD Inhibitor. Our goal was to increase drug exposure in liver (target organ) by engaging active transport into heptocytes via the liver-specific organic anion transporting polypeptides (OATPs). Our goal was to incorporate key transporting elements into SCD inhibitors to enable recognition by the OATP transport proteins while maintaining SCD potency. Moreover, we also sought to decrease the extent of unselective passive cell diffusion in order to minimize exposures in off-target tissues and cells (skin and eye). Fortunately, acidic moieties used to engage the active transporters generally impart reduced passive cell penetration. Nonetheless, we required a research operating procedure (ROP) that would allow us to funnel potential compounds and help us identify compounds which may exhibit a liver-targeting tissue distribution profile. The ROP to select for liver-targeted SCD inhibitors is depicted in Figure 1 and can be summarized as follows:

Scheme 3. Synthesis of MK-8245 (7)[a]

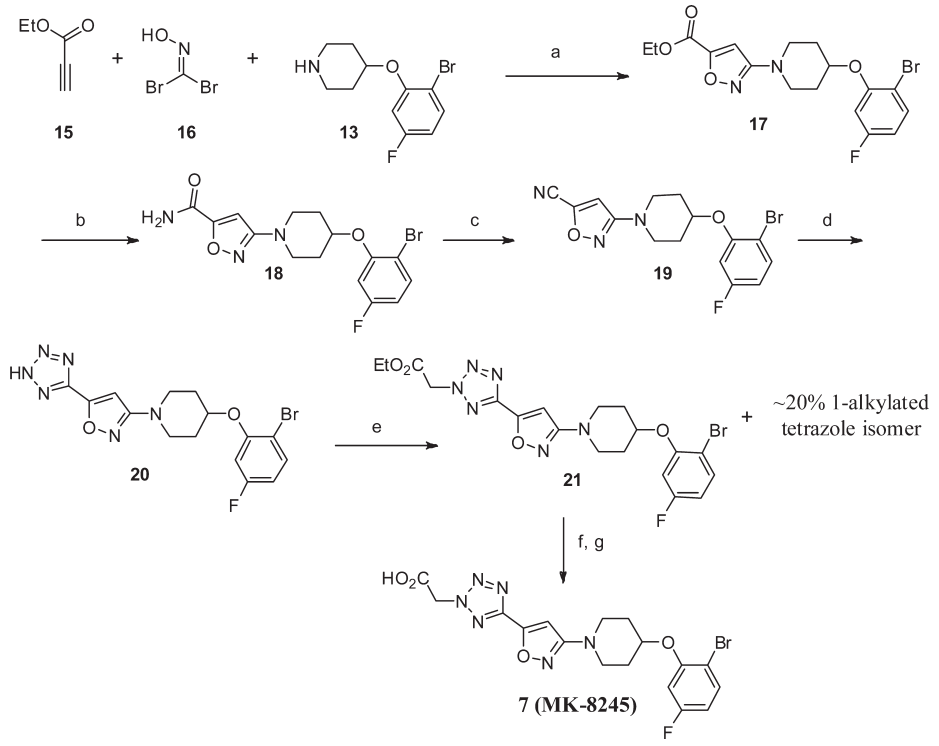

[a] Reagents and conditions: (a) $KHCO_3$, EtOAc, H_2O; (b) NH_4OH, MeOH, THF; (c) TFAA, Et_3N, CH_2Cl_2, 0 °C to rt; (d) NaN_3, py·HCl, NMP, 130 °C; (e) Et_3N, ethyl bromoacetate, THF, reflux; (f) NaOH, EtOH, H_2O; (g) HPLC separation.

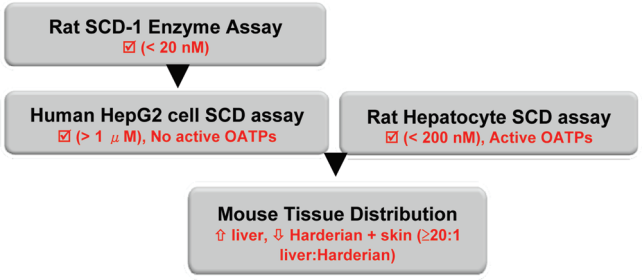

Figure 1. Strategy to identify liver-targeting SCD inhibitors. HepG2 cell SCD assay[21] is a gauge of the extent of passive cell diffusion; rat hepatocyte SCD assay identifies compounds which are actively transported into the liver; mouse tissue distribution is a measure of the extent of liver-targeting.

(i) determine if compounds are SCD inhibitors via an in vitro rat microsomal enzyme assay,[20] (ii) test active SCD inhibitors in two cell assays, one devoid of active OATPs (HepG2 cell line[21]) and one containing functional, active OATPs (rat hepatocyte), and (iii) conduct mouse tissue distribution studies on those compounds which are at least 4- to 5-fold more potent in the OATP vs non-OATP cell assays.

The first task was to determine where an acidic moiety could be appended onto existing SCD inhibitors to impart recognition by OATPs, decrease passive cell diffusion while at the same time maintaining SCD potency. Starting with our previously reported SCD inhibitor MF-438 (**1**) (Figure 2),[9] acidic moieties were placed on either the right- or left-hand side of the molecule. It became evident that acidic moieties were only tolerated on the left-hand side of the molecule (**2**, Figure 2); appendage of acids on the right-hand side produced compounds completely devoid of SCD inhibition (**3**, Figure 2). One of the first acidic moieties to be appended was the tetrazole (**4**, Scheme 1). This resulted in a significant loss of potency on the SCD1 rat enzyme (~140-fold, **4** vs **1**, Table 1) as well as being inactive in the HepG2 cell assay. However, compound **3** exhibited a modest SCD inhibition in the rat hepatocyte assay which contains active OATPs (IC_{50} = 3467 nM). This demonstrated that appendage of an acidic moiety could decrease passive cell penetration and engage in active transport into a hepatocyte (assumption based on HepG2 vs hepatocyte shift). To improve potency on the rat SCD enzyme assay, structure−activity relationship (SAR) studies were performed on the right-hand side phenoxy portion and, as has been previously reported,[22] 2,5-dihalogen substitution resulted in a significant 8-fold improvement in potency (**5**, rat enzyme IC_{50} = 34 nM, Scheme 2, Table 1). Compound **5** was significantly shifted in the HepG2 assay (370-fold) and slightly more potent in the hepatocyte assay (4-fold vs HepG2). A further increase in potency could be obtained by appending an acetic acid side chain onto the tetrazole heterocycle (**6**, rat enzyme IC_{50} = 7 nM, Table 1). In this case, the acidic tetrazole moiety was effectively replaced with a carboxylic acid. As with the tetrazoles **4** and **5**, acid **6** was >100-fold shifted in potency in the HepG2 cellular assay and more potent in the hepatocyte assay. Finally, by replacing the middle thiadiazole ring with an isoxazole (**7**, Scheme 3), the potency in both the rat enzyme and hepatocyte assays was further improved 2-fold (Table 1) while maintaining a >300-fold shift in the HepG2 assay. This compound is designated as **7** and was also determined to be a highly potent inhibitor of the human SCD1 enzyme (IC_{50} = 1 nM).[23] It should be also noted that for all of the SCD inhibitors listed in this paper,

dx.doi.org/10.1021/jm200319u | J. Med. Chem. 2011, 54, 5082–5096

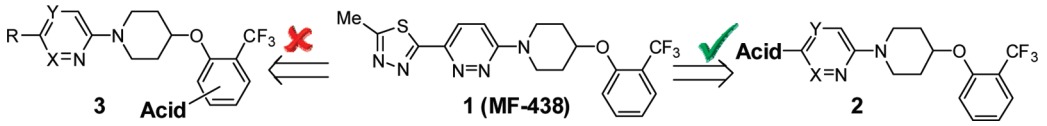

Figure 2. Chemical structure of systemically distributed **1**. Compounds of general structures **2** and **3** were assessed for potency vs the rat microsomal SCD1 enzyme.[20] Compounds of general structure **2** inhibited the rat SCD1 enzyme (IC_{50}s < 1 μM), whereas compounds of general structure **3** were inactive vs rat SCD1 (IC_{50}s > 10 μM).

Table 1. In Vitro Potencies and Liver-Targeting Tissue Distribution Profiles of Key SCD Inhibitors

	SCD inhibitor				
assay	**1**	**4**	**5**	**6**	**7**
rat microsomal enzyme IC_{50} (nM)[a,20]	2	276	34	7	3
Hum HepG2 Cell IC_{50} (nM)[a,21]	21	>50000	12588	904	1066
rat hepatocyte cell IC_{50} (nM)[a]	157	3467	3070	189	68
HepG2/hepatocyte ratio	0.14:1	>14:1	4:1	5:1	16:1
mouse [liver]/[Harderian gland] ratio[a,b]	1.5:1	330:1	26:1	40:1	21:1

[a] Data represent mean values of at least $n = 3$. [b] 6 h post 10 mg/kg PO dose.

there were no significant differences in potencies between the rat, mouse, and human SCD1 (i.e., for **7**, the rat, mouse, and human SCD1 enzyme IC_{50}s were 3, 3, and 1 nM, respectively). Moreover, all of the SCD inhibitors listed in Table 1 were highly selective over the Δ-5 and Δ-6 desaturases (i.e., >100000 μM vs rat and human Δ5D and Δ6D as assessed in the HepG assay[21]).

Liver-Targeted Tissue Distribution Profile. To determine if our strategy to select compounds based on their shift in the HepG2 vs hepatocyte assays resulted in compounds which exhibit a liver-targeted tissue distribution profile, the inhibitors in Table 1 were dosed in mice (10 mg/kg, PO) and 6 h post dose the animals were euthanized and the concentration of compound in select tissues (plasma, liver, skin, and the eye-lubricating Harderian glands) was measured. To simplify the discussion, the liver-to-Harderian gland ratio was used as a measure of the degree of liver-targeting. Starting with what we suspected to be a systemically distributed compound (i.e., a compound that distributes readily to most tissues), **1**, which is actually more potent in the HepG2 assay vs hepatocyte assay, did show almost equivalent levels of compound in the Harderian gland vs liver (Table 1). We were gratified to observe that the tetrazole **3**, which is at least 14-fold more potent in the hepatocyte vs HepG2 assay, did demonstrate a liver-targeted tissue distribution profile. As indicated in Table 1, the liver-to-Harderian gland ratio for **3** was >300:1, which is clearly superior to the 1.5:1 ratio obtained with the nonacidic compound **1**. Finally, the more potent acidic SCD inhibitors (**5**, **6**, and **7**) also demonstrated a liver-targeted tissue distribution profile as judged by their liver-to-Harderian gland ratios.

In addition to generating OATP substrate affinity, our liver-targeting strategy required the minimization of passive cell diffusion to prevent the penetration of any circulating SCD inhibitor to off-target tissues. The most potent SCD inhibitor **7** was significantly shifted in the non-OATP HepG2 cellular assay (~350-fold), indicating that this compound should possess the desired lack of cell penetration. To confirm this, the diffusion rate of **7** was evaluated across monolayers of LLC-PK1 cells and the P_{app} was determined to be 3.8×10^{-6} cm/s, which is indicative of poor to moderate cell penetration[24] (Supporting Information Method 2). It should be noted that we required the liver-targeting compound to be absorbed in the GI tract in order to be delivered to the portal vein effectively. Thus, there still had to be some degree of cell penetration (i.e., $P_{app} > 1 \times 10^{-6}$ cm/s and $<10 \times 10^{-6}$ cm/s) and it was determined that compound **7** was moderately bioavailable in multiple species (F = 12%, 28% and 40% in mice, rats and dogs, respectively). Moreover, it is known that OATPs are expressed in the intestinal wall[25,26] and this may also be responsible for the absorption of compound **7**.

To determine if mouse liver-targeting via OATPs would translate to liver-targeting in other species,[27] **7** was dosed orally to mice, rats, dogs, and rhesus monkeys and at 6 h post dose, the animals were euthanized, and the concentration of compound in select tissues (plasma, liver, skin, and Harderian glands) was measured. Only rodents possess Harderian glands, and because the corresponding eye-lubricating meibomian glands in dogs and rhesus monkeys were too difficult to extract, skin was used as the off-target tissue to measure liver-targeting in these higher species. As depicted in Figure 3, in all species examined, **7** was distributed mainly to the liver, with low exposure in tissues associated with potential adverse events (i.e., skin and eye lubricating glands). The liver-to-skin ratios were >30:1 in all four species.

OATP Transport Profile. To demonstrate that **7** is actively transported via human OATPs, uptake studies were performed in butyrate-treated stably transfected OATP1B1 and 1B3 MDCKII cell lines. As shown in Figure 4, **7** was found to be a substrate of both OATP1B1 and 1B3 and the uptake was inhibited by the OATP inhibitor sulfobromophthalein[28] (BSP). This data suggests OATP1B1 and OATP1B3 likely contribute toward the liver selectivity of **7** by mediating uptake into hepatocytes. The potency of **7** was measured in both freshly isolated and cryopreserved human hepatocytes and was found to be highly potent (IC_{50} = 5 nM, Supporting Information Method 3) compared to the non-OATP human HepG2 cell line (IC_{50} = 1066 nM), further indicating active uptake transport of **7** by human OATPs.

Pharmacological Efficacy of the Liver-Targeted SCD Inhibitor 7. To assess the diabetic efficacy, lipid efficacy, and safety profile of a systemically distributed vs liver-targeted SCD inhibitor, the following models were used: (i) acute oral glucose tolerance in eDIO mice (oGTT) to assess glucose clearance and (ii) chronic administration in eDIO mice to assess body weight

dx.doi.org/10.1021/jm200319u |J. Med. Chem. 2011, 54, 5082–5096

a

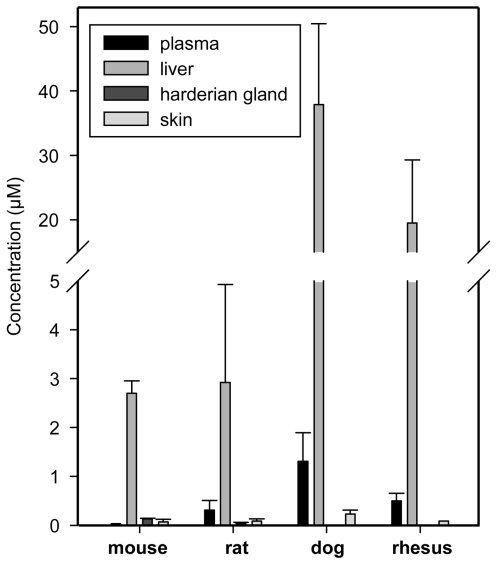

b

Species	[Liver]:[Plasma]	[Liver]:[Harderian gland]	[Liver]:[Skin]
Mouse	90:1	21:1	39:1
Rat	10:1	73:1	32:1
Dog	29:1	ND	164:1
Rhesus monkey	39:1	ND	217:1

Figure 3. Plasma and tissue concentration ratios at 6 h post oral dosing of **7** in mouse, rat, dog, and rhesus monkey. (a) Concentration of **7** in tissues 6 h post dose. Compound **7** was dosed orally (formulated in 0.5% methylcellulose) to male C57BL6 mice (n = 2, 10 mg/kg), male Sprague−Dawley rats (n = 3, 10 mg/kg), female rhesus monkeys (n = 2, 5 mg/kg), and male beagle dogs (n = 2, 5 mg/kg). (b) Ratio of tissue concentrations in liver vs tissues associated with potential adverse events. ND = not determined.

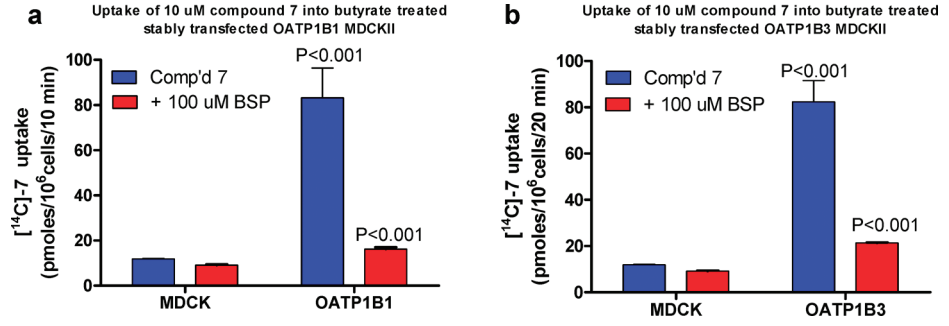

Figure 4. Uptake of **7** into (a) OATP1B1 stably transfected MDCK11 cells and (b) OATP1B3 stably transfected MDCK11 cells. OATP1B1 and 1B3 were found to mediate the BSP sensitive uptake of **7**, suggesting these transporters may play a role in the uptake of **7** into human hepatocytes. All data are mean ± sem, n = 3.

effects and lipid profile as well as evaluating the adverse event profiles in skin and eyes. Compounds **1** and **7** were given orally to eDIO mice 1 h before administration of an oral glucose challenge, and blood glucose levels were monitored for 2 h thereafter. As shown in Figure 5, both the systemically distributed **1** and the liver-targeted **7** improved glucose clearance dose-dependently to a similar extent, with ED_{50} values of 3 and 7 mg/kg, respectively. This was the first indication that selectively inhibiting liver SCD1 with a liver-targeted small molecule SCD inhibitor was effective at lowering glucose levels.

Chronic efficacy of the systemically distributed **1** and the liver-targeting SCD inhibitor **7** was evaluated in a 4-week oral dosing study in eDIO mice. Once-daily oral dosing was used for compound **1** based on its 6.4 h plasma half-life in mouse,[9] whereas bid dosing was required for **7** (mouse plasma half-life = 0.7 h) to provide similar SCD inhibition over the course of the experiment. Table 2 compares the mouse pharmacokinetics of compounds **1** and **7** and also indicates that the terminal trough liver levels of both compounds in the chronic eDIO mouse study are similar and would provide near complete liver SCD inhibition (see Supporting Information Results 2). As shown in Figure 6a, compound **1** treatment resulted in a significant, dose-dependent decrease in body weight (∼10% and 20% for the 1 and 5 mg/kg treatment groups, respectively), comparable to the effect seen with the CB1 inverse agonist AM251.[29] On the other hand, the liver-targeted inhibitor **7**, dosed at 20 or 60 mg/kg bid, showed only a modest prevention of body weight gain (∼5% BW gain reduction, Figure 6b). The maximally efficacious dose of **1**, based on body weight effects, was 5 mg/kg, qd. For compound **7**, the maximally efficacious dose was 20 mg/kg bid based on body weight and liver triglyceride reduction (60 mg/kg bid dose did not provide improved efficacy results). Histological analysis showed that hepatic steatosis was significantly reduced, which was confirmed by a reduction of liver triglyceride levels (see Supporting Information Results 3, Figure 3). In these eDIO studies, there was no effect on food consumption with either compound.

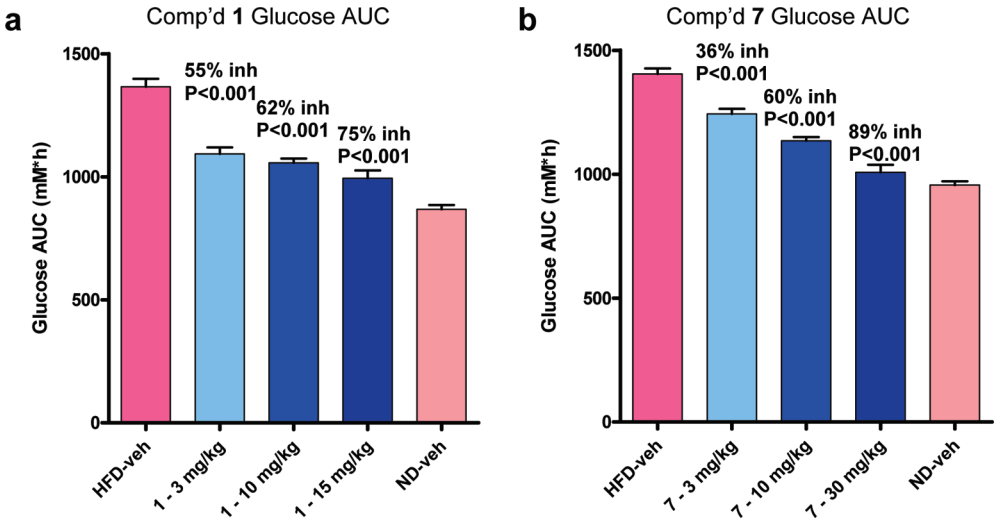

Figure 5. Dose-dependent effect of **1** and **7** on oGTT in DIO mice. Mice that were fed a high fat diet (HFD) for at least 14 weeks and had an established obesity state before the study were fasted for 16 h. Test compound was given 1 h before administration of oral glucose at 2 g/kg. (a) Compound **1** effect on glucose AUC following doses of 3, 10, and 15 mg/kg and (b) compound **7** effect on glucose AUC following doses of 3, 10, and 30 mg/kg. HFD, high fat diet; ND, normal diet; Veh, vehicle. n = 10−15 mice/group; mean ± sem.

Table 2. Mouse Pharmacokinetics of Compounds 1 and 7

	mouse pharmacokinetics[a]						
compd	Cl (mL/min/kg)	Vd (L/kg)	$t_{1/2}$ (h)	F (%)	plasma C_{max} (μM)	plasma AUC (μM·h)	trough liver levels from eDIO (μM)[b]
1[c]	15	7	6.4	73	1.3	19	5
7[d]	41	1	0.7	12	0.4	1	4

[a] Mouse PK parameters obtained following a 2 mg/kg IV and 10 mg/kg PO dose of compounds **1** and **7** to fasted male C57BL6 mice. Concentrations of compounds **1** and **7** were determined by LC-MS/MS and values represent the mean of n = 3 animals. [b] Liver concentrations were determined at trough at termination of the 4-week eDIO mouse study at the 20 mg/kg bid dose of compound **7** and the 5 mg/kg qd dose of compound **1**. [c] Compound **1** was dosed IV as a solution in 60%PEG-200 (5 mL/kg) and PO as a suspension in 1% methocel (10 mL/kg). [d] Sodium salt of compound **7** was dosed IV as a solution in saline (1 mL/kg) and PO as a suspension in 0.5% methocel (10 mL/kg).

Evaluation of Skin and Eye Adverse Effects in Rodents Treated with Systemic vs Liver-Targeted SCD Inhibitors. In addition to evaluating efficacy end points in the chronic 4-week eDIO mouse studies, comparison of the skin and eye adverse effect profiles of a systemic vs liver-targeted SCD inhibitor was of paramount importance. Notably, would a liver-targeted SCD inhibitor impart a therapeutic window compared to a systemically distributed inhibitor? As previously reported for systemically distributed SCD inhibitors,[8−10] both skin and eye abnormalities were observed in compound **1**-treated eDIO mice (Figures 7a,b). In contrast to systemically distributed SCD inhibitors, which induce significant skin and eye adverse effects in the eDIO mouse within 5−10 days of treatment at therapeutic doses, the liver-targeted **7** did not induce meaningful skin or eye adverse events during the 4-week treatment period (Figures 7c, d). To confirm that the improved adverse event profile observed with **7** in the 4-week eDIO mouse study is due to lack of SCD inhibition in the off target tissues, the desaturation indices (DIs) in the off-target tissues were compared to that obtained in the liver. The DI is the ratio of SCD product-to-SCD substrate ([C18:1, oleic acid]/[C18:0, stearic acid]) and is a direct measure of chronic SCD activity.[13] A reduction in DI indicates inhibition of the SCD enzyme and DI can be monitored in plasma and tissues. For the systemically distributed **1** at a maximally efficacious dose of 5 mg/kg qd, the liver SCD DI was reduced by ∼56% (Figure 8a, not significant due to high variation in vehicle-treated mice), while there was significant reduction of SCD activity in both the Harderian gland (92% ↓ DI, Figure 8b) and skin (25% ↓ DI, Figure 8c). These significant DI reductions are consistent with the high exposure of **1** in all of these tissues ([liver] = 10 μM, [Harderian gland] = 5 μM, [skin] = 4 μM).

In contrast, for the liver-targeted SCD inhibitor **7**, while there was very significant reduction in liver DI (63%) following 4 weeks of dosing 20 mg/kg bid in eDIO mice, there was no significant reduction in Harderian gland DI (Figures 8d,e, respectively; skin DI was not measured in the compound **7**-treated mice). The reduction of DI (liver) or lack thereof (Harderian gland) was consistent with the exposure of **7** in these tissues ([liver] = 5 μM, [Harderian gland] = 0.9 μM). It should be noted that there was a small erosion of liver-targeting upon chronic dosing of **7** as assessed by liver-to-Harderian gland ratio (21:1 following single administration vs 5:1 after 4 weeks of dosing). The liver-to-Harderian gland ratio for **7** reached steady state (5:1) after ∼1 week of dosing, did not worsen upon chronic dosing (4 weeks) and was sufficient in providing a therapeutic window in the chronic eDIO mouse model (i.e., lack of harderian gland SCD inhibition (Figure 8e) and no significant eye AEs (Figure 7d)).

One of most well-documented classes of liver-targeting small-molecule therapeutics are HMG-CoA reductase inhibitors (statins). As with SCD inhibitors, distribution of statins to tissues other than liver is linked to adverse events (myopathy in the case of statins).[30] Statins are liver-targeted by virtue of their affinity for the liver-specific organic anion transporting polypeptides (OATPs),

dx.doi.org/10.1021/jm200319u |J. Med. Chem. 2011, 54, 5082–5096

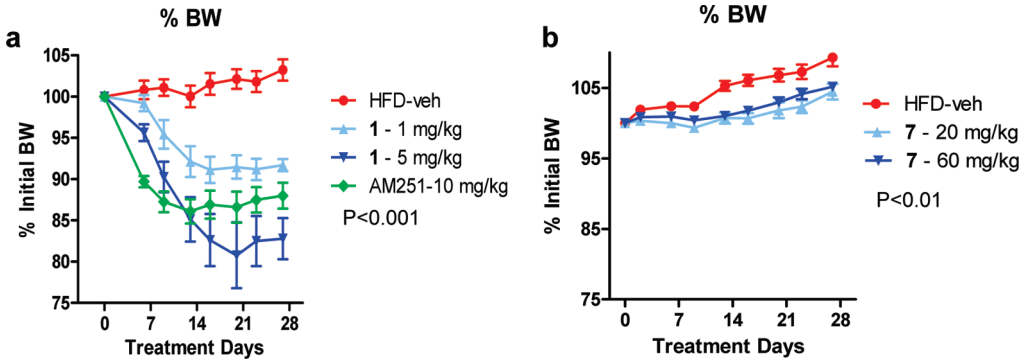

Figure 6. Effect on body weight following chronic dosing of (a) **1** vs (b) **7** in eDIO mice. eDIO mouse fed on HFD for at least 18 weeks prior to initiation of study were dosed orally with vehicle, **1** (1 or 5 mg/kg, qd) or **7** (20 or 60 mg/kg, bid). Doses were selected to target sustained liver SCD inhibition based on mouse liver PD results (Supporting Information Method 4). HFD, high fat diet; Veh, vehicle; $n = 8-10$ mice/group; mean ± sem.

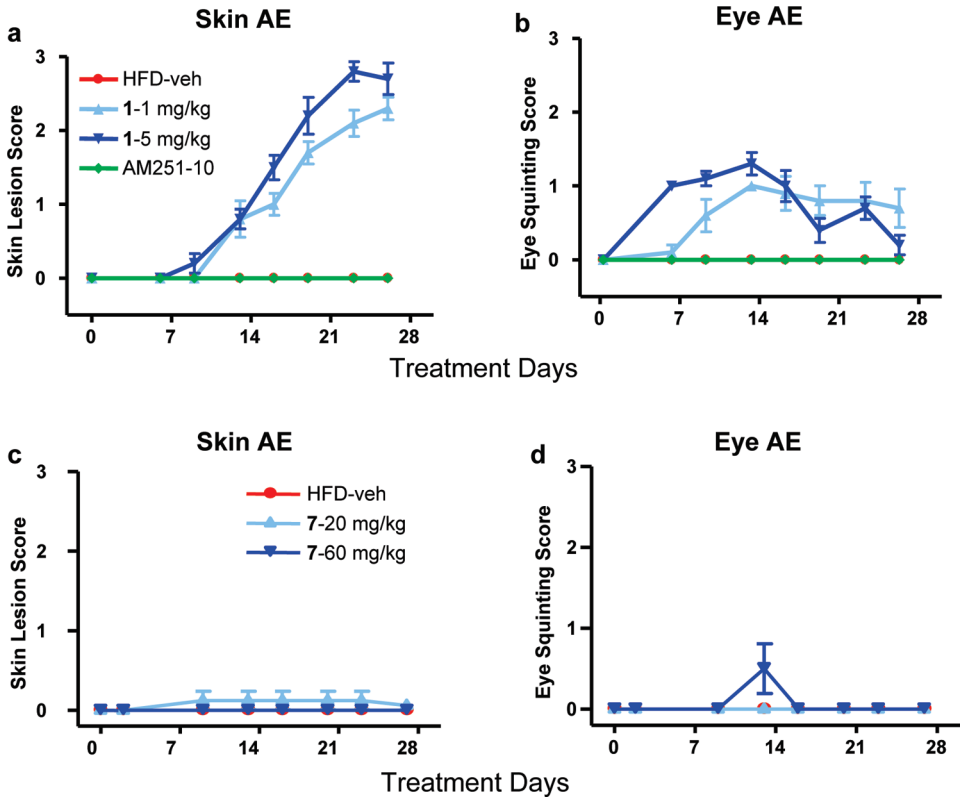

Figure 7. Skin and eye adverse event profile of **1** (a and b) and **7** (c and **d**) in a 4-week eDIO mouse study. Skin scoring system: 0, normal; 1, small patch (1−3 mm) of hair loss; 2, larger patch (3− 0 mm); 3, extensive patch with lesions. Eye scoring system: 0, normal; 1, squinting eye; 2, partial eye closure, one eye; 3, both eyes closed. To lessen the severity and allow for completion of the study, eye lubrication (BNP: Neomycin and Polymyxin B Sulfates and Bacitracin Ophthalmic Ointment, USP) was applied to the eyes of compound **1**-treated mice starting on day 12. Veh = vehicle.

and it was strategized that targeting the same OATP transporters would lead to the generation of a liver-targeted SCD inhibitor. The fact that statins were substrates for the OATPs was not known a priori and this liver-targeting feature was not knowingly designed into the compounds to improve the therapeutic index. In fact, realization that statins were OATP substrates occurred after the first statin was already on the market. It was the goal of our research efforts to implement an in vitro strategy to predict the liver-targeting capabilities of a compound.

Transporters can affect the tissue distribution of drugs and thereby contribute to the selective distribution of drugs to specific tissues. Two of the OATP transporters (1B1 and 1B3) are specifically expressed in the liver, are localized to the basolateral membrane of the hepatocytes, and facilitate the uptake of drugs from the blood into hepatocytes.[31] Drug substrates of OATPs 1B1 and 1B3 include a large number of structurally diverse compounds, such as statins (i.e., atorvastatin, rosuvastatin, simvastatin acid, etc.), endothelin receptor antagonists (i.e., atrasentan), certain antibiotics (i.e., benzylpenicillin), and angiotensin II receptor antagonists (i.e., olmesartan, valsartan), just to name a few.[31] One of the key structural features that these drugs have in common is an acidic moiety, either a

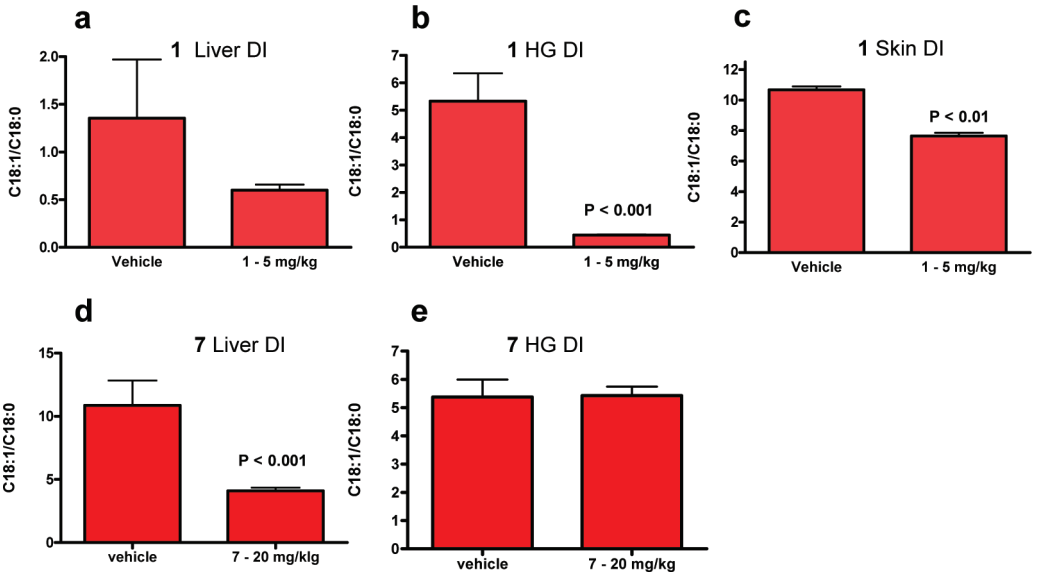

Figure 8. Desaturation indices in tissues of eDIO mice treated with **1** or **7**. eDIO mice fed on HFD for at least 18 weeks prior to initiation of study were dosed orally with vehicle, **1** (5 mg/kg, qd, 3 days) or **7** (20 mg/kg, bid, 28 days). Following sacrifice, tissues were harvested and DI measurements were obtained. (a and d) represent liver DI measurements in vehicle vs **1** or **7**-treated mice, respectively; (b and e) represent Harderian gland (HG) DI measurements in vehicle vs **1** or **7**-treated mice, respectively; (c) represents skin DI measurements in vehicle vs **1**-treated mice (skin DI for **7**-treated mice was not determined). $n = 8-10$ mice/group; mean ± sem.

carboxylic acid or tetrazole moiety. It was determined that adding an acidic moiety to the left-hand side of systemically distributed SCD inhibitors allowed for retention of SCD potency (compounds **4**, **5**, **6**, and **7**, Table 1). However, simply adding an acidic moiety on the left-hand side of the molecule did not automatically impart recognition by the liver-specific OATPs, as judged by the shift in potency in HepG2 vs hepatocyte assays as well as in tissue distribution studies. Detailed SAR studies regarding the correct positioning of the acidic moiety to maximize both SCD potency and liver-targeting will be the subject of subsequent publications.

The optimization of liver-targeted SCD inhibitors depicted in Table 1 involved the important use of the HepG2 and hepatocyte SCD cellular assays. The principle reason for using cellular SCD assays to gauge OATP substrate affinity is that they are very high throughput. Assays to directly measure OATP substrate affinity certainly exist (see Experimental Section) but are not sufficiently high throughput to be able to test hundreds of compounds per month. The goal of the HepG2 assay is to gauge the extent of passive diffusion and compounds which are not potent in this assay are desired to minimize diffusion and distribution to non-liver tissues. Conversely, in the OATP hepatocyte cell assay, compounds which are recognized by the OATPs will be actively transported into the hepatocyte and should be more potent at inhibiting intracellular SCD compared to the HepG2 assay. It should be noted that there is only a loose correlation between HepG2-to-hepatocyte potency shift and liver-targeting as measured by compound levels in mouse liver vs Harderian gland. However, as depicted in Table 1, HepG2/hepatocyte ratios of ≥4 do translate to significant and likely sufficient liver-targeting as determined from the mouse tissue distribution analyses. In the tissue distribution analysis, particular attention is focused on the drug concentration in tissues where adverse events have been observed in the *SCD1*$^{-/-}$ mice (the eye lubricating Harderian gland and skin tissue). Focusing only on the plasma-to-liver ratio can be misleading because many nontransported drugs reach high concentrations in the liver due to rapid exchange of blood constituents with the liver tissue. Drugs absorbed in the gastrointestinal tract are completely transported to the liver via the portal vein, and after steady state has been reached, most compounds do not demonstrate cell specificity (liver levels of compound vs that in other tissues). For example, the liver-to-plasma ratios for the systemically distributed **1** and the liver-targeted compound **4** were very similar (14:1 for **1** vs 15:1 for **4**) and could not be used to discriminate these two compounds. However, when comparing the liver-to-Harderian gland ratios, there is clearly a difference (1.5:1 for **1** and >300:1 for **4**), thereby demonstrating the need to examine drug concentrations in the off-target tissues to properly assess liver targeting. Our target tissue distribution profile was determined to be a concentration of drug in liver that fully inhibits SCD and that is at least 20-fold higher than levels found in the off-target tissues (Harderian gland and skin). The most potent liver-targeted SCD inhibitor **7** met these criteria not only in mouse but also in rat, dog, and rhesus monkey. Furthermore, compound **7** is likely to be liver-targeted in humans due to the fact that it was found to be a substrate for the human OATP1B1 and 1B3 (Figure 4) and was also very potent in a human hepatocyte assay (IC_{50} = 5 nM). It has been reported that there is a strong association between simvastatin-induced myopathy and two tightly linked variants of the OATP1B1 gene.[32] This is likely due to impaired liver uptake of simvastatin in those subjects with the OATP1B1 variants which, in turn, leads to increased systemic exposure of the statin and adverse events in the off target muscle tissue. The fact that **7** is actively taken up in the liver by both OATP1B1 and OATP1B3 may mitigate the risk of skin and eye adverse events in patients with the OATP1B1 variants. Nonetheless, the effect of OATP1B1 polymorphisms and tolerability of compound **7** will be followed up in the future with in vitro uptake tools and in clinical studies.

It was shown in Figure 5 that the liver-targeted inhibitor **7** was as efficacious in the oGTT eDIO mouse model as the systemically distributed **1**. In an attempt to understand the mechanism by which hepatic SCD1 inhibition results in an improved oral glucose tolerance in eDIO mice, a hyperinsulinemic−euglycemic glucose clamp experiment in overfed rats was carried out (see Supporting Information Results 1). As shown in Supporting Information Figure 1a, under hyperinsulinemic−euglycemic conditions, compound **7** significantly increased the glucose infusion rate (GIR) required to maintain euglycemia, indicative of improvement in whole body insulin sensitivity. This was accompanied by a nonsignificant suppression in hepatic glucose production (Supporting Information Figure 1b). These results indicate that a liver-targeted small molecule SCD inhibitor (**7**) improves whole body insulin sensitivity, consistent with the literature report with a liver-targeted ASO against SCD1.[6] In a chronic eDIO mouse model, there were differences in efficacy and tolerability noted between the systemically distributed SCD inhibitor **1** and the liver-targeted **7**. While efficacy on liver triglyceride and liver steatosis was similar for **1** and **7**, the effect on body weight reduction was significantly different (20% vs 5%, respectively, Figure 6). It is clear that the antiobesity effect with liver-selective SCD inhibitors is very modest compared to that obtained with systemically distributed inhibitors. In an attempt to understand the obesity efficacy differences, the liver-targeted SCD1 inhibitor **6** and the systemically distributed SCD1 inhibitor **1** were compared head-to-head in the eDIO mouse model and the following parameters were measured: (i) body weight and (ii) inhibition of SCD activity (DI) in fat vs liver tissues. As previously observed in Figure 6, the systemically distributed SCD inhibitor **1** had a significant body weight loss (∼15%) vs vehicle-treated mice whereas the liver-targeted SCD inhibitor **6** did not promote significant body weight loss in eDIO mice (see Supporting Information Results 4, Figure 4a). Both **1** and **6** had similar inhibition of liver desaturation index (DI = [C18:1]/[C18:0], direct measure of chronic SCD activity) at termination of the 2-week study, indicating that similar levels of liver SCD inhibition had been obtained (Supporting Information Figure 4b). Conversely, while there was significant inhibition of eWAT DI for compound **1**, there was no inhibition observed in eWAT for the liver-targeted **6** (Supporting Information Figure 4c), which confirms that liver-targeting prevents exposure of SCD compounds to other tissues. This data suggests that robust obesity efficacy likely requires inhibition of adipose SCD and is in agreement with previously reported data.[4]

With regards to tolerability and adverse event profile in the chronic eDIO mouse studies, there were important differences between the systemically distributed SCD inhibitor **1** and the liver-targeted inhibitor **7**. As reported in parts a and b of Figure 7, compound **1** induced eye adverse events, followed a few days later by skin adverse events. At the maximally efficacious dose of **7** (20 mg/kg bid), there was observed a liver-targeted tissue distribution profile which correlated with liver TG efficacy (Supporting Information Figure 3a), modest body weight loss and ***no*** significant eye or skin adverse events during the course of the 4-week study (Figures 7c,d). At a 3-fold higher dose of **7** (60 mg/kg bid), a clean adverse event profile was also observed, which indicates that a therapeutic window could be obtained by targeting the SCD inhibitor to the liver, consistent with reported SCD1 gene intervention studies.[4,5] The greatly improved AE profile observed with the liver-targeted SCD inhibitor **7** was consistent with no significant inhibition of SCD in the off-target tissue as assessed by monitoring the DI in the Harderian gland following chronic dosing in the eDIO mouse model (Figure 8e). The level of DI reduction in the liver and Harderian gland in this chronic study correlated with the high drug exposures of **7** in the liver and the lower drug exposure in skin and eye. This indicated that the liver-targeting SCD inhibitor **7** was successful at providing good SCD inhibition in liver while sparing inhibition in tissues associated with adverse events.

CONCLUSION

In this report, a liver-targeting strategy was successfully implemented which resulted in the discovery of **7**, a potent, liver-targeted SCD inhibitor with excellent in vitro and preclinical in vivo efficacy. This approach utilized high throughput cellular assays, which predicted the extent of liver-specific OATP substrate affinity. Following confirmation of liver-targeting by tissue distribution studies, the lower throughput OATP assays could be used to confirm human OATP substrate affinity. While liver-targeting OATP approaches have been used to improve the therapeutic window of pharmaceutical agents such as statins, to the best of our knowledge, this is the first report of how to intentionally design a liver-targeting agent via OATP substrate affinity. Liver-targeting allowed compound **7** to demonstrate maximal liver SCD inhibition while sparing inhibition in the skin and eye tissues associated with adverse events. This ultimately resulted in an improved safety profile for the liver-targeted SCD inhibitor **7** relative to the previously reported systemically distributed inhibitor **1**. Future studies involve the clinical evaluation of **7** for the treatment of diabetes and dyslipidemia.

EXPERIMENTAL SECTION

General. All commercial chemicals were used without further treatment. Anhydrous solvents were purchased from Sigma-Aldrich (Milwaukee, WI), Acros Organics (Fisher Scientific, Nepeau, ON, Canada), or American Chemicals Ltd. (Montreal, QC, Canada). TLC analyses were performed on Merck 60 F_{254} silica gel glass-backed plates, with spots detected visually under ultraviolet irradiation (254 nm). Purification of the crude reaction mixtures was performed as indicated using chromatography on silica gel using a CombiFlash apparatus (Teledyne Isco, Lincoln, NE) equipped with columns of appropriate size (Teledyne Isco, Lincoln, NE, or Silicycle, Québec City, QC, Canada). Proton (^{1}H NMR) magnetic resonance spectra were recorded on a Bruker AM instrument operating at 400 or 500 MHz. All spectra were recorded using residual solvent ($CHCl_3$, acetone or DMSO) as internal standard. Signal multiplicity was designated according to the following abbreviations: s = singlet, d = doublet, dd = doublet of doublets, t = triplet, m = multiplet, br s = broad singlet, br t = broad triplet. Carbon (^{13}C NMR) nuclear magnetic resonance spectra were recorded on a Bruker AM instrument operating at 126 MHz. All spectra were recorded using residual solvent ($CHCl_3$ or DMSO) as internal standard. High-resolution mass spectrometry (HRMS) was performed in the ESI mode using an Agilent Technologies MSD TOF mass spectrometer coupled to an Agilent Technologies 1200 series LC. All melting points were determined on a Buchi 510 melting point apparatus in open capillary tubes and are uncorrected. Chemical purity of compounds was assessed by reversed-phase HPLC and all compounds were determined to have ≥95% purity. Reversed-phase HPLC purity determinations were performed at three different wavelengths (λ_{max}, 220 and 254 nm) on an Agilent Technologies 1100 series system equipped with a Zorbax RxC18 column (150 mm × 4.6 mm, 5 μ) using an acetonitrile/water gradient containing 0.1% formic acid. Reactions

were carried out with continuous stirring under a positive pressure of dry nitrogen except where noted. The synthesis of **1** is described in reference.[9]

*4-[2-(Trifluoromethyl)phenoxy]piperidine Hydrochloride (**8**).* To a solution of *tert*-butyl 4-hydroxypiperidine-1-carboxylate (25 g, 124 mmol), 2-hydroxy-benzotrifluoride (22 g, 136 mmol) and triphenylphosphine (39 g, 149 mmol) in THF (250 mL) was added diethyl azodicarboxylate (23.5 mL, 149 mmol) dropwise at 0 °C. The mixture was then warmed to room temperature and stirred for 14 h. The mixture was concentrated and diluted with Et_2O, washed with 1 N NaOH and water, and then dried over Na_2SO_4. The mixture was concentrated and diluted with Et_2O/hexanes (35:65). The solid was filtered, and the filtrate was concentrated. The residue was purified by column chromatography on silica gel (eluting with 35% Et_2O/hexanes) to give *tert*-butyl 4-[2-(trifluoromethyl)phenoxy]-piperidine-1-carboxylate as a solid. Trifluoroacetic acid (26.3 mL, 342 mmol) was added to a solution of *tert*-butyl 4-[2-(trifluoromethyl)phenoxy]piperidine-1-carboxylate (29.5 g, 85 mmol) in CH_2Cl_2 (171 mL). The mixture was stirred at room temperature for 16 h. The solvent was evaporated. The residue was diluted with EtOAc (200 mL), washed with 2 N NaOH (3 × 100 mL), brine, dried over Na_2SO_4, and evaporated to give 4-(2-trifluoromethyl)-phenoxy)piperidine as an oil (21.3 g, 70% yield). The corresponding hydrochloride (title compound) can be prepared by precipitation of an ethereal solution (0.5−1M) of the free amine with 1 equiv of 4N HCl in dioxane. ^{1}H NMR (400 MHz, DMSO-d_6) δ 9.20 (br, 2H), 7.58−7.61 (m, 2H), 7.32−7.34 (t, 1H), 7.06−7.08 (t, 1H), 4.87−4.90 (m, 1H), 3.06−3.08 (m, 4H), 1.92−2.14 (m, 2H), 1.81−1.91 (m, 2H); (m/z): $(M + H)^+$ 246.

*5-{4-[2-(Trifluoromethyl)phenoxylpiperidin-l-y1}-1,3,4-thiadiazol-2-amine (**10**).* To a solution of 4-[2-(trifluoromethyl)phenoxylpiperidine hydrochloride (**8**) (5.5 g, 19.5 mmol) in DMF (50 mL) was added 5-bromo-1,3,4-thiadiazol-2-amine (**9**) (3.3 g, 18.3 mmol) and K_2CO_3 (9.1 g, 65.8 mmol). The reaction was heated at 80 °C with stirring overnight. After cooling, the salt was removed by filtration and the filtrate was evaporated in vacuo. The residue was triturated with EtOAc to afford the title compound (4.4 g, 70% yield). ^{1}H NMR (400 MHz, DMSO-d_6): δ 7.57−7.60 (m, 2H), 7.29−7.35 (m, 1H), 7.03−7.05 (m, 1H), 6.46 (s, 2H), 4.84 (br s, 1H), 3.22−3.30 (m, 4H), 1.91−2.01 (m, 2H), 1.68−1.78 (m, 2H); (m/z): $(M + H)^+$ 345.

*5-{4-[2-(Trifluoromethyl)phenoxy]piperidin-1-yl}-1,3,4-thiadiazole-2-carbonitrile (**11**).* To a suspension of 5-{4-[2-(trifluoromethyl)phenoxy]-piperidin-1-yl}-1,3,4-thiadiazol-2-amine (**10**) (10.0 g, 29.0 mmol) in CH_3CN (150 mL) was added CuCN (5.3 g, 59.2 mmol) and *t*-BuONO (90%) (8 mL, 60.0 mmol) at room temperature. The reaction mixture was heated at 50−60 °C for 2 h until TLC indicated disappearance of the starting material. The reaction mixture was diluted with EtOAc and mixed with silica gel. The resulting suspension was filtered through a pad of silica gel by eluting with 100% EtOAc. The filtrate was concentrated in vacuo to afford the crude product, which was purified by column chromatography on silica gel (eluting with 2:1 hexanes/EtOAc) to afford the title compound (4.2 g, 41% yield) as a yellow oil. ^{1}H NMR (400 MHz, $CDC1_3$): δ 7.61 (d, 1H), 7.50 (t, 1H), 6.93−7.06 (m, 2H), 4.86 (br s, 1H), 3.77−3.83 (m, 4H), 2.01−2.20 (m, 4H); (m/z): $(M + H)^+$ 355.

*1-[5-(2H-Tetrazol-5-yl)-1,3,4-thiadiazol-2-yl]-4-[2-(trifluoromethyl)-phenoxy]-piperidine (**4**).* A suspension of 5-{4-[2-(trifluoromethyl)-phenoxy]piperidin-1-yl}-1,3,4-thiadiazole-2-carbonitrile (**11**) (4.99 g, 14.1 mmol), NaN_3 (4.65 g, 71.5 mmol), and pyridinium hydrochloride (3.43 g, 29.7 mmol) in NMP (50 mL) was heated at 130 °C for 18 h. The reaction mixture was cooled to room temperature and poured into aqueous 0.5 N HC1, extracted with EtOAc, and washed three times with aqueous 0.5 N HC1 and with aqueous brine solution. The organic layer was dried (Na_2SO_4) and filtered. Evaporation of the solvent was followed by trituration in a mixture of MeOH/Et_2O/heptane (1:1:6) (v/v) with stirring for 4 h at room temperature. After this time, the suspension was cooled with an ice−water bath, and the title compound (**4**) was collected by filtration as a white solid (4.77 g, 85% yield). The material was dried under high vacuum by heating at 50 °C for 1−2 h; mp 226−228 °C. ^{1}H NMR (400 MHz, DMSO-d_6): δ 7.60−7.62 (m, 2H), 7.37 (d, 1H, J = 9.0 Hz), 7.08 (t, 1H, J = 7.5 Hz), 4.86−4.95 (m, 1H), 3.56−3.64 (m, 4H), 2.00−2.15 (m, 2H), 1.75−1.89 (m, 2H). ^{13}C NMR (126 MHz, DMSO-d_6): δ 173.3, 155.1, 149.7 (broad peak), 143.3, 134.7, 127.5 (q, J_{CF} = 5.1 Hz), 124.3 (q, J_{CF} = 272 Hz), 120.9, 118.2 (q, J_{CF} = 29.4 Hz), 115.1, 71.6, 47.1 (2C), 29.4 (2C). HRMS (ESI) (m/z): $(M + H)^+$ calcd for $C_{15}H_{15}F_3N_7OS$, 398.1005; found, 398.0997.

*5-Bromo-1,3,4-thiadiazole-2-carbonitrile (**12**).* To a suspension of ethyl 5-amino-1,3,4-thiadiazole-2-carboxylate (10 g, 58 mmol) in CH_3CN (180 mL) was added $CuBr_2$ (25.7 g, 115 mmol). The mixture turned dark green and was further stirred for 15 min at room temperature. *t*-BuONO, 90% (13.8 mL, 115 mmol) was added dropwise over 15−20 min. The mixture became slightly warm, and gas was evolved after 5 min and then throughout the addition. After completion of the addition and gas evolution subsided, the mixture was heated at 60 °C for 30 min. Solvent was then evaporated in vacuo. Water and EtOAc were added, and the mixture was agitated in the flask until the dark-green color disappeared. The organic phase became light brown, and the aqueous was green with insoluble material. The whole mixture was filtered through Celite and washed with EtOAc. The EtOAc layer was separated, washed with dilute brine solution, dried (Na_2SO_4), and concentrated to give ethyl 5-bromo-1,3,4-thiadiazole-2-carboxylate (13.5 g, 98% yield). ^{1}H NMR (400 MHz, acetone-d_6): δ 4.52 (q, 2H), 1.43 (t, 3H). To a solution of ethyl 5-bromo-1,3,4-thiadiazole-2-carboxylate (13.5 g, 56.9 mmol) in THF (50 mL) at room temperature was added NH_4OH (28 wt %, 39.6 mL, 164 mmol). The mixture was stirred at room temperature overnight, and a precipitate appeared in the aqueous layer. Volatile materials were removed in vacuo. The mixture was diluted with water and the precipitate was collected, washed with water, and dried under vacuum to afford 5-bromo-1,3,4-thiadiazole-2-carboxamide (9.3 g, 79% yield). ^{1}H NMR (400 MHz, acetone-d_6): δ 7.99 (s, 1H), 7.55 (s, 1H). To a solution of 5-bromo-1,3,4-thiadiazole-2-carboxamide (11 g, 53 mmol) and Et_3N (17.1 mL, 122 mmol) in THF (106 mL) at 0 °C was added TFAA (17 mL, 58 mmol). The mixture was then warmed to room temperature and stirred for 30 min. Solvent was evaporated in vacuo. The residue was diluted with water. The precipitate was collected, washed with water, and dried to give the title compound (7 g, 70% yield). ^{13}C NMR (75 MHz, $CDC1_3$): δ 77.3, 109.0, 141.7.

*4-(2-Bromo-5-fluorophenoxy)piperidine (**13**).* To a solution of *tert*-butyl 4-hydroxypiperidine-l-carboxylate (50.6 g, 251 mmol) and di-*tert*-butyl azodicarboxylate (71.0 g, 308 mmol) in THF (350 mL) was added 2-bromo-5-fluorophenol (36 mL, 324 mmol). The mixture was cooled to −78 °C, and a solution of triphenylphosphine (81.5 g, 311 mmol) in CH_2C1_2 (130 mL) was added via a cannula. The reaction was then warmed to room temperature and stirred overnight. The solvents were removed under vacuum, and the crude oil was dissolved in EtOH (200 mL). The solution was cooled to −78 °C and treated with 4 M HC1 in 1,4-dioxane (450 mL). The reaction was warmed to room temperature and stirred 24 h. After this time, the solvents were removed under vacuum. The salts were neutralized with 1 N NaOH (750 mL) and extracted with a mixture of Et_2O:hexanes (1:1) several times. The organic layers were combined and concentrated to dryness. The crude material was treated with heptane (1 L), and a white precipitate was filtered and discarded. The heptane layer was diluted with Et_2O and treated with 4 M HC1 in 1,4-dioxane (100 mL). The resulting precipitate was collected by filtration and washed three times with Et_2O:hexanes (1:1). The salts were again neutralized with 1 N NaOH (500 mL) and extracted with a mixture of Et_2O:hexanes (1:1) several times. The organic layers were combined, washed with brine, dried ($MgSO_4$), filtered, and concentrated. The crude material was dissolved

in heptane (2 L), washed four times with 1 N NaOH (250 mL) and brine, and dried ($MgSO_4$). The organic layer was filtered and concentrated to dryness to afford the title product as a colorless oil (54 g, 78% yield). ^{1}H NMR (500 MHz, acetone-d_6): δ 7.58 (dd, 1H), 7.00 (dd, 1H), 6.70 (td, 1H), 4.64−4.58 (m, 1H), 3.12−3.06 (m, 2H), 2.73−2.66 (m, 2 H), 2.02−1.94 (m, 2H), 1.69−1.60 (m, 2H).

*5-[4-(2-Bromo-5-fluorophenoxy)piperidin-1-yl]-1,3,4-thiadiazole-2-carbonitrile (**14**).* To a solution of 4-(2-bromo-5-fluorophenoxy)-piperidine (**13**) (14.4 g, 52.7 mmol) in 1,4-dioxane (80 mL) was added *N*,*N*-diisopropylethylamine (20 mL, 115 mmol), followed by 5-bromo-1,3,4-thiadiazole-2-carbonitrile (**12**) (10.0 g, 52.7 mmol). The mixture was stirred 1 h at room temperature. The reaction mixture was then poured into saturated aqueous NH_4C1, extracted with EtOAc, washed with brine, dried (Na_2SO_4), filtered, and concentrated under reduced pressure. The crude material was purified by column chromatography on silica gel (eluting with a gradient from 10 to 40% EtOAc/hexanes) to afford the desired product as a colorless oil (15.6 g, 77% yield). ^{1}H NMR (500 MHz, acetone-d_6): δ 7.63 (dd, 1H), 7.14 (dd, 1H), 6.78 (td, 1H), 5.04−4.99 (m, 1H), 4.00−3.95 (m, 2H), 3.89−3.84 (m, 2H), 2.27−2.21 (m, 2H), 2.11−2.05 (m, 2H).

*4-(2-Bromo-5-fluorophenoxy)-1-[5-(2>H-tetrazol-5-yl)-1,3,4-thiadiazol-2-yl]piperidine (**5**).* A suspension of 5-[4-(2-bromo-5-fluorophenoxy)piperidin-l-y1]-1,3,4-thiadiazole-2-carbonitrile (**14**) (15.6 g, 40.7 mmol), NaN_3 (13.2 g, 204 mmol), and pyridinium hydrochloride (9.47 g, 82.0 mmol) in NMP (70 mL) was heated at 130 °C for 4 h. The reaction mixture was cooled to room temperature and poured into aqueous 0.5 N HC1, extracted with EtOAc, and washed three times with aqueous 0.5 N HC1 and with aqueous brine solution. The organic layer was dried (Na_2SO_4) and filtered. Evaporation of the solvent was followed by trituration in a mixture of MeOH/Et_2O/heptane (1:1:6) (v/v). After filtration of the solid, the material was triturated again in this solvent system to finally afford the desired product (**5**) as a white solid (15.3 g, 88% yield); mp: 213-215 °C. ^{1}H NMR (400 MHz, acetone-d_6): δ 7.64 (dd, 1H, J = 9.0, 6.5 Hz), 7.16 (dd, 1H, J = 9.0, 3.0 Hz), 6.79 (td, 1H, J = 9.0, 3.0 Hz), 5.04−5.00 (m, 1H), 4.02−3.94 (m, 2H), 3.89−3.81 (m, 2H), 2.29−2.20 (m, 2H), 2.12−2.03 (m, 2H). ^{13}C NMR (126 MHz, DMSO-d_6): δ 173.3, 162.8 (d, J_{CF} = 243 Hz), 154.6 (d, J_{CF} = 10.9 Hz), 149.7 (broad peak), 143.3, 134.2 (d, J_{CF} = 10.0 Hz), 109.6 (d, J_{CF} = 22.7 Hz), 107.5 (d, J_{CF} = 3.0 Hz), 104.2 (d, J_{CF} = 26.4 Hz), 72.8, 47.2 (2C), 29.4 (2C). HRMS (ESI) (m/z): $(M + H)^+$ calcd for $C_{14}H_{14}BrFN_7OS$, 428.0122; found, 428.0131.

*(5-{5-[4-(2-Bromo-5-fluorophenoxy)piperidin-1-yl]-1,3,4-thiadiazol-2-yl}-2H-tetrazol-2-yl)acetic Acid (**6**).* A solution of 4-(2-bromo-5-fluorophenoxy)-1-[5-(2*H*-tetrazol-5-yl)-1,3,4-thiadiazol-2-yl]piperidine (**5**) (4.54 g, 10.66 mmol) in DMF (20 mL) was treated with NaH (60% in oil) (512 mg, 12.80 mmol) at −78 °C. The mixture was warmed to 0 °C for 10−15 min, cooled again to −78 °C, and ethyl bromoacetate (1.6 mL, 14.37 mmol) was added dropwise. The final reaction mixture was warmed and stirred at room temperature overnight. The reaction mixture was poured into aqueous 1 N HCl and extracted with EtOAc. The organic layers was washed with 1 N HCl and brine, dried (Na_2SO_4), and filtered. Solvents were removed in vacuo to afford the crude product, which was purified by column chromatography on silica gel (eluting with a gradient from 10 to 50% EtOAc/hexanes). The two isomers were triturated with a mixture of Et_2O/heptane. The more polar isomer (R_f = 0.3 (50% EtOAc/hexanes)), obtained as an off-white solid (2.60 g, 48% yield), was the desired isomer ethyl (5-{5-[4-(2-bromo-5-fluorophenoxy)piperidin-1-yl]-1,3,4-thiadiazol-2-yl}-2*H*-tetrazol-2-yl)acetate. ^{1}H NMR (500 MHz, DMSO-d_6): δ 7.64 (dd, 1H), 7.29 (dd, 1H), 6.82 (td, 1H), 5.98 (s, 2H), 4.93−4.89 (m, 1H), 4.24 (q, 2H), 3.84−3.77 (m, 2H), 3.72−3.66 (m, 2H), 2.13−2.06 (m, 2H), 1.901.83 (m, 2H), 1.24 (t, 3H).

The less polar isomer (R_f = 0.5 (50% EtOAc/hexanes)), obtained as a white solid (2.55 g, 47% yield), was ethyl (5-{5-[4-(2-bromo-5-fluorophenoxy)piperidin-1-yl]-1,3,4-thiadiazol-2-yl}-1*H*-tetrazol-1-yl)-acetate. ^{1}H NMR (500 MHz, DMSO-d_6): δ 7.64 (dd, 1H), 7.29 (dd, 1H), 6.82 (td, 1H), 5.79 (s, 2H), 4.94−4.89 (m, 1H), 4.19 (q, 2H), 3.86−3.80 (m, 2H), 3.75−3.69 (m, 2H), 2.12−2.06 (m, 2H), 1.901.84 (m, 2H), 1.20 (t, 3H).

To a solution of ethyl (5-{5-[4-(2-bromo-5-fluorophenoxy)-piperidin-1-yl]-1,3,4-thiadiazol-2-yl}-2*H*-tetrazol-2-yl)acetate (2.57 g, 5.02 mmol) in a mixture of THF/MeOH (30 mL) (2:1) (v/v) was added 1 N NaOH (10 mL) at room temperature. After 5 min, the reaction mixture was poured into 1 N HCl, extracted with EtOAc, washed with brine, dried (Na_2SO_4), filtered, and concentrated. The residue was triturated with a mixture of Et_2O/hexanes to give the desired material (**6**) as a white solid (2.23 g, 92% yield); mp: 243−245 °C (decomp). ^{1}H NMR (400 MHz, DMSO-d_6): δ 13.89 (br s, 1H), 7.65 (dd, 1H, J = 8.8, 6.3 Hz), 7.30 (dd, 1H, J = 9.0, 3.0 Hz), 6.83 (td, 1H, J = 9.0, 3.0 Hz), 5.84 (s, 2H), 4.95−4.88 (m, 1H), 3.86−3.78 (m, 2H), 3.74−3.66 (m, 2H), 2.15−2.07 (m, 2H), 1.92−1.84 (m, 2H). ^{13}C NMR (126 MHz, DMSO-d_6): δ 172.8, 167.6, 162.8 (d, J_{CF} = 244 Hz), 158.3, 154.6 (d, J_{CF} = 10.7 Hz), 144.8, 134.3 (d, J_{CF} = 9.9 Hz), 109.6 (d, J_{CF} = 22.6 Hz), 107.5 (d, J_{CF} = 4.3 Hz), 104.2 (d, J_{CF} = 26.8 Hz), 72.8, 54.5, 47.2 (2C), 29.4 (2C); the regioconfiguration of the acetic acid moiety was assigned by a ^{15}N gHMBC experiment (J_{HN} = 5 Hz) on the sodium salt of **5** with observation of three long-range couplings between the methylene protons at δ 5.00 ppm and tetrazole nitrogens at δ 393.8, 314.9, and 303.0 ppm (^{15}N-benzamide external ref δ 110 ppm) and was confirmed by X-ray crystallography. HRMS (ESI) (m/z): $(M + H)^+$ calcd for $C_{16}H_{16}BrFN_7O_3S$, 486.0178; found, 486.0182.

*Ethyl 3-[4-(2-bromo-5-fluorophenoxy)piperidin-1-yl]isoxazole-5-carboxylate (**17**).* To a suspension of 4-(2-bromo-5-fluorophenoxy)-piperidine (**13**) (20 g, 73 mmol), hydroxycarbonimidic dibromide (**16**) (13 g, 64 mmol), and ethyl propiolate (**15**) (38 g, 422 mmol) in EtOAc/H_2O (390 mL/65 mL) was added $KHCO_3$ (19.4 g, 194 mmol). The mixture was stirred for 12 h at room temperature. The organic layer was then separated, dried over anhydrous Na_2SO_4, and concentrated. Chromatography over silica gel and elution with hexanes/EtOAc (1:1) and swishing in hexanes/Et_2O (3:2) to give the title compound as a white powder (5.0 g, 19% yield). ^{1}H NMR (400 MHz, acetone-d_6): δ 7.62 (dd, 1H), 7.11 (dd, 1H), 6.97 (s, 1H), 6.76 (td, 1H), 4.91−4.86 (m, 1H), 4.39 (q, 2H), 3.71−3.63 (m, 2H), 3.49−3.41 (m, 2H), 2.17−2.09 (m, 2H), 1.99−1.88 (m, 2H), 1.38 (t, 3H).

*3-[4-(2-Bromo-5-fluorophenoxy)piperidin-1-yl]isoxazole-5-carboxamide (**18**).* To a suspension of ethyl 3-[4-(2-bromo-5-fluorophenoxy)-piperidin-1-yl]isoxazole-5-carboxylate (**17**) (2.0 g, 4.84 mmol) in MeOH (10 mL) and THF (10 mL) was added ammonium hydroxide (28 wt %, 20 mL, 144 mmol) at room temperature. The mixture was stirred at room temperature overnight stirring. A precipitate appeared after about 15 min and became more abundant after overnight. Volatile materials were then removed in vacuo. The residue was diluted with water and extracted with EtOAc. The EtOAc extract was washed with diluted brine, dried (Na_2SO_4), and concentrated. The residue was triturated in Et_2O/hexanes (1:1) to give the title compound as a white powder (1.7 g, 91% yield). ^{1}H NMR (400 MHz, acetone-d_6): δ 7.62 (dd, 1H), 7.52 (s, 1H), 7.11 (m, 2H), 6.80−6.71 (m, 2H), 4.91−4.85 (m, 1H), 3.69−3.61 (m, 2H), 3.46−3.38 (m, 2H), 2.17−2.09 (m, 2H), 1.99−1.88 (m, 2H).

*3-[4-(2-Bromo-5-fluorophenoxy)piperidin-1-yl]isoxazole-5-carbonitrile (**19**).* Trifluoroacetic anhydride (0.8 mL, 5.7 mmol) was added to a suspension of 3-[4-(2-bromo-5-fluorophenoxy)piperidin-1-yl]isoxazole-5-carboxamide (**18**) (1.6 g, 4.2 mmol) and Et_3N (1.5 mL, 10.8 mmol) in CH_2Cl_2 (20 mL) at ice−water bath temperature. After addition was completed, the cooling bath was removed and the mixture was stirred at room temperature for 2 h. The mixture was quenched with water (10−15 mL), followed by saturated $NaHCO_3$ (15−20 mL), and extracted with CH_2Cl_2 (2 × 30 mL). The combined CH_2Cl_2 extracts

were washed with diluted brine (40 mL), dried (Na_2SO_4), and concentrated. Chromatography over silica gel and elution with hexanes/EtOAc (4:1) gave the title compound as a colorless gum (1.4 g, 92% yield). ^{1}H NMR (400 MHz, acetone-d_6): δ 7.62 (dd, 1H), 7.33 (s, 1H), 7.10 (dd, 1H), 6.76 (td, 1H), 4.93−4.86 (m, 1H), 3.71−3.63 (m, 2H), 3.52−3.44 (m, 2H), 2.18−2.09 (m, 2H), 1.99−1.90 (m, 2H).

*4-(2-Bromo-5-fluorophenoxy)-1-[5-(1H-tetrazol-5-yl)isoxazol-3-yl]-piperidine (**20**).* A mixture of 3-[4-(2-bromo-5-fluorophenoxy)piperidin-1-yl]isoxazole-5-carbonitrile (**19**) (1.4 g, 3.82 mmol), pyridine hydrochloride (0.9 g, 7.79 mmol), and sodium azide (1.3 g, 20.00 mmol) in NMP (12 mL) was stirred and heated at 130 °C bath for 2 h. After cooling, the mixture was diluted with water and acidified with 1 N HCl to precipitate the tetrazole. The whole mixture was then extracted with EtOAc. The EtOAc extract was washed three times with water, dried (Na_2SO_4), and concentrated. The residue was triturated with Et_2O to give the title compound as a light-brown powder (1.4 g, 89% yield). ^{1}H NMR (400 MHz, acetone-d_6): δ 7.63 (dd, 1H), 7.12 (m, 2H), 6.76 (td, 1H), 4.93−4.88 (m, 1H), 3.77−3.69 (m, 2H), 3.55−3.47 (m, 2H), 2.21−2.13 (m, 2H), 2.02−1.92 (m, 2H).

*Ethyl (5-{3-[4-(2-bromo-5-fluorophenoxy)piperidin-1-yl]isoxazol-5-yl}-2H-tetrazol-2-yl)acetate (**21**).* A mixture of 4-(2-bromo-5-fluorophenoxy)-1-[5-(1*H*-tetrazol-5-yl)isoxazol-3-yl]piperidine (**20**) (1.2 g, 2.93 mmol), ethyl bromoacetate (0.45 mL, 4.04 mmol), and Et_3N (0.75 mL, 5.38 mmol) in THF (12 mL) was refluxed for 2 h. After cooling, the mixture was diluted with water and extracted with EtOAc. The EtOAc extract was washed with water, dried (Na_2SO_4), and concentrated. The crude material was purified by column chromatography on silica gel (Combi-Flash apparatus, 40 g SiO_2 column, eluting with 25−40% EtOAc in hexanes for 20 min, 35 mL/min, 18 mL/fraction) to give the title compound as a colorless gum (1.1 g, 76% yield), also containing about 20% of the positional isomer ethyl (5-{3-[4-(2-bromo-5-fluorophenoxy)piperidin-1-yl]isoxazol-5-yl}-1*H*-tetrazol-1-yl)acetate. ^{1}H NMR (400 MHz, acetone-d_6): δ 7.63 (dd, 1H), 7.14−7.09 (m, 1H), 7.03 (s, 1H), 6.76 (td, 1H), 5.84 (s, 2H), 4.93−4.87 (m, 1H), 4.34−4.26 (m, 2H), 3.77−3.68 (m, 2H), 3.55−3.46 (m, 2H), 2.21−2.12 (m, 2H), 2.03−1.91 (m, 2H), 1.30 (t, 3H).

*(5-{3-[4-(2-Bromo-5-fluorophenoxy)piperidin-1-yl]isoxazol-5-yl}-2H-tetrazol-2-yl)acetic acid (**7**).* A mixture of ethyl (5-{3-[4-(2-bromo-5-fluorophenoxy)piperidin-1-yl]isoxazol-5-yl}-2*H*-tetrazol-2-yl)acetate (**21**), containing about 20% of the positional isomer ethyl (5-{3-[4-(2-bromo-5-fluorophenoxy)piperidin-1-yl]isoxazol-5-yl}-1*H*-tetrazol-1-yl)-acetate (0.175 g, 0.354 mmol) in EtOH (2 mL) and 1 M NaOH solution, (1.77 mL, 1.77 mmol) was stirred at room temperature for 3 h. Volatile solvents were removed in vacuo. The residue was diluted with water, acidified with 1 M HCl, and extracted with dichloromethane. The combined organic layers were dried over anhydrous Na_2SO_4, filtered, and concentrated to give the crude product, which was purified by preparative HPLC. HPLC conditions were: (a) column: YMC-Pack ODS-AQ 250 mm × 20 mm; (b) eluant: solvent A, acetonitrile with 0.075% TFA, and solvent B, water with 0.075% TFA; gradient: 0−15 min, 44% A in B to 74% A in B, then 15−18 min; 74% A in B to 100% A. The title compound (**7**) was obtained from the fraction eluting at about 15.5 min (0.083 g, 50% yield); mp: 204.1 ± 0.9 °C. ^{1}H NMR (500 MHz, DMSO-d_6): δ 13.90 (s, 1H), 7.60 (dd, J = 8.8, 6.3 Hz, 1 H), 7.25−7.19 (m, 2 H), 6.77 (td, J = 8.5, 2.7 Hz, 1 H), 5.83 (s, 2 H), 4.82−4.78 (m, 1 H), 3.59−3.53 (m, 2 H), 3.43−3.33 (m, 2 H), 2.03−1.97 (m, 2 H), 1.78−1.71 (m, 2 H). ^{13}C NMR (126 MHz, DMSO-d_6): δ 167.6, 167.2, 162.8 (d, J_{CF} = 244 Hz), 157.8, 155.8, 154.7 (d, J_{CF} = 10.8 Hz), 134.2, (d, J_{CF} = 10.0 Hz), 109.5 (d, J_{CF} = 22.7 Hz), 107.5 (d, J_{CF} = 3.7 Hz), 104.1 (d, J_{CF} = 26.6 Hz), 97.4, 73.4, 54.5, 44.2 (2C), 29.3 (2C); the regioconfiguration of the acetic acid moiety was assigned by a ^{15}N gHMBC experiment (J_{HN} = 5 Hz) with observation of three long-range couplings between the methylene protons at δ 5.83 ppm and tetrazole nitrogens at δ 386.2, 305.5, and 282.3 ppm (^{15}N-benzamide external ref δ 110 ppm). In comparison, the regioconfiguration of the acetic acid moiety of the nondesired isomer of **7** was assigned by a similar ^{15}N gHMBC experiment with observation of two long-range couplings between methylene protons at δ 5.66 ppm and tetrazole nitrogens at δ 374.8 and 228.1 ppm and was further corroborated by observation of strong NOE between the methylene protons and isoxazole proton in a 1D ROESY experiment (mix = 500 ms). HRMS (ESI) (m/z): $(M + H)^+$ calcd for $C_{17}H_{17}BrFN_6O_4$, 469.0455; found, 469.0455.

Rat SCD Hepatocyte Assay. Male Sprague−Dawley rats were fed a high carbohydrate diet (Ren's Feed & Supplies Ltd. no. 7576) for 2 days to obtain SCD1-induced liver (175−200 g). Rat hepatocytes were isolated by collagenase perfusion. Cells were plated, 100 μL of 4 × 10^6 cells/mL cells per well on a 96-well plate (NUNC). Then 1.2 μL of compound was added to each well and incubated for 15 min at 37 °C/5% CO_2. Then 20 μL of ^{14}C-stearic acid (final concentration 0.5 μCi/ml) was added and incubated for 1 h, shaking in an Eppendorf shaker set at 400 rpm with 37 °C/5% CO_2. Hepatocytes were spun down and washed three times with PBS buffer to remove the tracer in medium. Complete hydrolysis was done by incubation at 75 °C for 1 h with 2N NaOH. Cell lysate was acidified with phosphoric acid and then the lipids were extracted with acetonitrile. The quantification of the resulting radiolabeled oleic acid and stearic acid in the final organic phase was done by HPLC, using a C18-reverse phase column (Zorbax extended C18 (4.6 mm × 75 mm), eluting with a 3% water (0.1% formic acid)/acetonitrile to 100%. Acetonitrile gradient (0.1% formic acid) at a flow rate of 2 mL/min in 4 min, detection via a Packard Flow scintillation analyzer.

Tissue Distribution Analysis Method. Compound **7** was administered orally to fed C57BL6 mice (n = 2), male Sprague−Dawley rats (n = 3), female rhesus monkeys (n = 2), or fasted male beagle dogs (n = 2) using 0.5% methylcellulose as vehicle and 6 h post dose, the animals were sacrificed, tissues were harvested, and the concentration of **7** in tissues was analyzed following the procedure outlined below.

For Mice and Rats. Requested tissues (less than 0.2 g) were weighed and put in a blue 96-well plate for tissues (strips of 12, attached, 1.1 mL microtubes in microracks from National Scientific Supply Co.) and frozen at −78 °C. Tissues were thawed and diluted with 3.5 volumes of a 2.5:1 MeCN:H_2O mixture containing internal standard. To this mixture was added 125−150 mg of silicon carbide chips and a small (4 mm) stainless steel bead (bead must be added to the 96-well plate prior to the addition of the tissue). The 96-well plate was capped (Marsh bio plug caps, polyethylene for microtubes, strips of 12) and shaken at 1500−1700 strokes per min using a GenoGrinder for 20 min. The plate was then centrifuged for 15 min and the supernatant was transferred to a mass spec vial and the concentration of **7** was determined by LC-MS. Quantification involved the preparation of a standard curve using blank plasma instead of tissue (i.e., 10 μL of blank plasma +10 μL of MeCN (with internal standard) containing different concentrations of **7** + 10 μL of water + 15 μL of MeCN (with internal standard). Because of the small size of mouse Harderian glands (i.e., ∼10 mg/gland), a similar procedure was used, except 2 volumes of water and 4 volumes of acetonitrile were added to the well containing the Harderian gland (final concentration was adjusted based on increased initial dilution). For skin, tissue homogenization was not performed with the GenoGrinder. Instead, to an 8 mL vial containing a weighed piece of shaved skin was added 3.5 volumes of a 2.5:1 MeCN:H_2O mixture containing internal standard. The skin was then homogenized using a tissue tearor from Biospec Products Inc., followed by centrifugation and analysis as above.

For Dogs and Rhesus Monkeys. Liver and skeletal muscle samples (approx 1 g) were processed by hand using a tissue tearor from Biospec Products Inc. Four spatially separated pieces of liver lobe (1 g) were obtained during necropsy and processed separately. The results represent the average of the four samples, and all four samples were found to be within ±2-fold of the average. All skin and eyelid samples (approx 1 g)

were first frozen under liquid nitrogen and pulverized by hand with a hammer to a fine powder. The pieces were transferred and accurately weighted into a vial and diluted with 3.5 volumes of a 2.5:1 MeCN:H_2O mixture containing internal standard and further processed using the tissue tearor. The suspensions were then centrifuged, and the concentration of **7** in the supernatant was quantified using LC-MS.

OATP1B1 and OATP1B3 Recombinant Cell Line Uptake Assays. MDCKII cells were provided by Dr. A. H. Schinkel (The Netherlands Cancer Institute) and were used under license agreement. OATP1B1 (*SLCO1B1*) and OATP1B3 (*SLCO1B3*) cDNAs were amplified from human liver cDNA libraries (A. Demartis, IRBM, and R. Stocco, Merck Frosst, Montreal). OATP1B1 was cloned into the expression vector pcDNA3.1-hygro (Invitrogen, CA) and stably transfected into MDCKII cells (originally provided by Dr. P. Borst, The Netherlands Cancer Institute). OATP1B3 was cloned into the pcDNA5/FRT vector (Invitrogen) and stably transfected into Flp-In MDCKII cells (MDCKII cells stably transfected with Flp Recombinase Target site). MDCKII cell line was cultured in 96-well transwell culture plates (Millipore, MA). Five μM [^{14}C]-**7** (see Synthesis in Supporting Information Method 1) was prepared in HBSS with 10 mM HEPES. Substrate solution (150 μL) was added to either the apical (A) or the basolateral (B) compartment of the culture plate, and buffer (150 μL) was added to the compartment opposite to that containing the compound. At t = 3 h, 100 μL of sample was taken out from both sides and scintillant (5 mL, ReadySafe, Beckman Coulter, CA) was added. Radioactivity was determined by liquid scintillation counting in a LS6500 multipurpose liquid scintillation counter (Beckman Coulter, CA). [^{3}H]Prazosin (5 μM) was used as the positive control. The experiment was performed in triplicate.

The B−A/A−B ratio was calculated by dividing the P_{app} from B to A by the P_{app} from A to B at t = 3 h:

$$\text{B} - \text{A}/\text{A} - \text{B ratio} = \frac{P_{app}(\text{B} \rightarrow \text{A})}{P_{app}(\text{A} \rightarrow \text{B})}$$

OATP1B1 and OATP1B3 mediated uptake was determined in MDCKII cells stably transfected with OATP1B1 or OATP1B3 cDNAs. Twenty-four hours prior to the experiment, cells were treated with 10 mM sodium butyrate (Sigma-Aldrich, St. Louis, MO) to increase OATP expression. Cells were dislodged with trypsin EDTA (Invitrogen) and resuspended in HBSS with 10 mM Hepes, pH 7.4. Cells were then suspended in 96 deep well plates at a density of 0.2−0.6 × 10^6 cells/well. Uptake was initiated by the addition of the indicated concentrations of [^{14}C]-**7** or the positive control substrates [^{3}H]$E_2$17βG (for OATP1B1 studies) or [^{3}H]CCK8 (for OATP1B3 studies) in HBSS. Cells were incubated for the indicated time at 37 °C, then uptake was stopped, followed by immediate centrifugation at 1800g at 4 °C (Eppendorf, model 5180R; Hamburg, Germany) and washing of the cell pellets with phosphate buffered saline (PBS, Invitrogen), three times. Cell pellets were resuspended in 50% acetonitrile (Sigma-Aldrich), scintillation fluid was added (Scintisafe Econo 2; Fisher Chemicals, NJ) and radioactivity was determined by liquid scintillation counting in a LS6500 multipurpose scintillation counter (Beckman Coulter, CA). The experiment was performed in triplicate.

For uptake studies stably transfected MDCKII cells, data were expressed in nmoles × 10^{-1}/10^6 cells and pmol/10^6 cells, respectively. For uptake studies into membrane vesicles, data were expressed in pmol/mg protein. For substrate kinetic determinations, the transporter mediated component was calculated by subtracting uptake into parental cells from transporter expressing cells. This transporter mediated component was analyzed by nonlinear regression analysis in order to determine K_m data, using Prism 4.0 (Graphpad, San Diego, CA). Data in Figure 4 are mean ± SE.

The uptake of [^{14}C]-**7** (10 μM) into MDCKII cells stably transfected with the human uptake transporters OATP1B1 or OATP1B3 was time-dependent (data not shown) and significantly higher than in the control MDCKII cells (Figure 4a,b). OATP1B1 and OATP1B3 mediated uptake of [^{14}C]-**7** (10 μM) was significantly inhibited by bromosulphothalein (BSP), a known inhibitor of OATP transporters. Uptake of 1 μM [^{3}H]$E_2$17βG (OATP1B1 studies) or 10 nM [^{3}H]CCK8 (OATP1B3 studies) confirmed the functionality of these assays.

oGTT Study in eDIO Mice with 1 and 7. Male C57/Bl6 mice were fed a high fat diet (Bio-Serv F3283) for at least 14 weeks starting at 6 weeks of age. The obese mice were fasted for 16 h, and the SCD inhibitors **1** and **7** were given orally to eDIO mice 1 h before administration of oral glucose (2 g/kg). Blood glucose levels were monitored at t = −60 min, 0 min, 20 min, 40 min, 60 and 120 min post glucose challenge.

Chronic eDIO Mouse Studies with 1, 7, and 6. Male C57/Bl6 mice were fed a high fat diet (Bio-Serv F3283) for at least 18 weeks starting at 6 weeks of age. One week prior to dosing of compound, the eDIO mice were dosed with vehicle (1% methocel, bid) for 7 days. Prior to initiation of the study, the mice were randomized according to body weight, and on day 1, the mice were dosed either with vehicle, SCD inhibitor, or positive control (AM251[29]) (n = 8−10/group). Dosing continued for either 28 days (**1** and **7**, parts a and b of Figure 6) or 14 days (**1** and **6**, Figure 4 in Supporting Information Results 4). Body weight, food consumption, and skin and eye tolerability were monitored twice per week. Becaue of dry eyes, mice treated with compound **1** were administered eye lubrication (Neomycin and Polymyxin B Sulfates and Bacitracin Ophthalmic Ointment, USP, sterile: active ingredients per g Bacitracin Zinc 400 IU, Neomycin Sulfate (equivalent to 3.5 mg of neomycin base) 5 mg and Polymyxin B Sulfate 5000 IU) daily from day 12 onward to allow for completion of study (hence why the severity of reported eye abnormalities in Figure 7b diminished after day 12). At termination of the study, animals were euthanized and plasma and tissues (liver, skin, eWAT, Harderian glands) were collected for desaturation index measurements, determination of SCD inhibitor concentration, and triglyceride/steatosis measurements (liver only).

Method for Tissue Desaturation Index Determination. Liver, fat, Harderian gland, eWAT, and skin were collected for desaturation index determination. Liver, fat, eWAT, and Harderian glands were weighed and collected in strips of 12 attached microtubes in microracks (National Scientific, Claremont, California). Enough cold Dulbecco's Phosphate Buffer Saline (DPBS; Cellgro, Manassas, Virginia) was added to liver and fat to obtain a final concentration of 25 mg/100 μL. A fixed amount of 100 μL of cold DPBS was added to the Harderian glands. Three medium size (5/32″) stainless steel beads (MetalFini, St-Laurent, Québec) were added for homogenization. All tissues were mechanically milled using the GenoGrinder 2000 (ATS Scientific, Burlington, Ontario). Tough tissues like skin could not be properly homogenized using a GenoGrinder. Pieces of weighed shaved skin were collected in microcentrifuge tubes. The fresh or cryopreserved skin tissues were then transferred to 8 mL glass tubes. Enough 10N NaOH (J.T. Baker, Phillipsburg, New Jersey) was added to obtain a final concentration of 25 mg/500 μL. The skin samples were then hydrolyzed overnight at 100 °C. Upon cooling, 500 μL of hydrolyzed skin were transferred to new 8 mL glass tubes. Aliquots (100 μL) of fresh or cryopreserved liver, fat, eWAT, and Harderian gland tissue homogenates were also hydrolyzed by transferring them to 8 mL glass tubes (VWR), adding 500 μL of 10N NaOH, and submitting them to 100 °C for 1 h. Once cooled to room temperature, 1 mL of isooctane (Sigma-Aldrich, Milwaukee, Wisconsin) was added to all samples to conduct the first extraction. Samples were mixed thoroughly and centrifuged to separate the isooctane layer from the aqueous lower phase. The top layers of isooctane containing the undesirable lipids were removed and discarded. The surface of the aqueous phase was washed by gently adding 500 μL of isooctane on the side of the tube. Again, this isooctane was removed and

discarded. Samples were acidified to pH 2.0 by adding 700 μL of formic acid (Acros Organics, Geel, Belgium) and mixed. The extraction of the fatty acids was carried on by adding 500 μL of isooctane and thoroughly mixing. The solvent layers of isooctane containing the fatty acids were collected after centrifugation and transferred to new 8 mL glass tubes containing 1 mL of saturated NaCl solution with 1% formic acid. The purpose of this step is to remove all residual aqueous solution from the isooctane before gas chromatography (GC) analysis. Once mixed and centrifuged, an aliquot of 100 μL was transferred to GC vials (Chromatographic Specialties, Brockville, Ontario), containing 300 μL conical inserts with springs (Fisher Scientific, Ottawa, Ontario). The fatty acids were derivatized to their corresponding methyl esters with 20 μL of diazomethane solution prepared in-house and analyzed on an Agilent Technologies (Mississauga, Ontario) 6890N GC system equipped with a flame ionization detector (FID) using a HP-88 column (100 m length, 0.25 mm ID, 0.2 μM film), also from Agilent Technologies. Samples (2 μL) were injected in split mode using ratio up to 25:1. Helium was used as carrier gas at a flow rate of 2 mL/min. Hydrogen, provided by a Parker hydrogen generator (Cleveland, Ohio), was used as auxiliary gas for the flame ionization detector. The injector and detector temperatures were set at 250 and 280 °C, respectively. The initial oven temperature was set at 120 °C, increased to 165 °C at a rate of 10 °C/min, increased to 210 °C at a rate of 5 °C/min, and increased to 230 °C at a rate of 5 °C/min.

Data analysis of the fatty acid methyl esters (FAMEs) was done using the Agilent ChemStation integration software. FAMEs identification was achieved by comparison of retention times with those obtained from standard mixtures (NU-CHEK-PREP, Elysian, Minnesota). The Desaturation Index was determined by calculating the SCD-1 product peak area/SCD-1 substrate peak area.

Statistical Method. The *P* values reported in all figures were calculated using Merck CMG (comparing multiple groups) StatServer version 2.93, all pairwise comparisons, confidence intervals at 95%.

■ ASSOCIATED CONTENT

Supporting Information. The synthesis of [^{14}C]-radiolabeled **7**; the method for Papp determination; the human SCD hepatocyte assay method; the mouse liver SCD pharmacodynamic (PD) assay method; mouse liver triglyceride and steatosis analysis methods; the rat hyperinsulenemic-euglycemic glucose clamp method and results for **7**; mouse liver PD results for **1** and **7**; mouse liver triglyceride and steatosis results for **7**; chronic eDIO mouse study with **1** and **6**. This material is available free of charge via the Internet at http://pubs.acs.org.

■ AUTHOR INFORMATION

Corresponding Author

*Phone: (604) 484-3336. Fax: (604) 484-3459. E-mail: renataoballa@dhanni.com.

■ ACKNOWLEDGMENT

We thank Jingchao Dong, Dejun Liu, and Gaoyun Xie at WuXi AppTec for preliminary work on the synthesis of **7**.

■ ABBREVIATIONS USED

SCD1, stearoyl-CoA desaturase-1; OATPs, organic anion transporting polypeptides; C16:1, palmitoleic acid; C16:0, palmitic acid; C18:1, oleic acid; C18:0, stearic acid; ASO, antisense oligonucleotide; BMI, body mass index; AE, adverse event; mRNA, messenger ribonucleic acid; LKO, liver-specific knockout; siRNA, small interfering ribonucleic acid; ROP, research operating procedure; HepG2, human hepatocellular carcinoma cell line; SAR, structure−activity relationship; LLC-PK1, renal epithelial cell line originally derived from porcine kidneys; MDCKII, Madin−Darby canine epithelium kidney cell line; BSP, sulfobromophthalein; eDIO, established diet-induced obesity; oGTT, oral glucose tolerance test; CB1, cannabinoid receptor 1; DI, desaturation index; HMG-CoA reductase, 3-hydroxy-3-methyl-glutaryl-CoA reductase; eWAT, epididymal white adipose tissue; TG, triglyceride; AUC, area under the curve; HFD, high fat diet; ND, normal diet; veh, vehicle; ^{1}H NMR, proton nuclear magnetic resonance; ^{13}C NMR, carbon nuclear magnetic resonance; PBS, phosphate buffer solution; ND, not determined

■ REFERENCES

(1) Ntambi, J. M.; Miyazaki, M. Regulation of stearoyl-CoA desaturases and role in metabolism. *Prog. Lipid Res.* **2004**, *43*, 91–104.

(2) Ntambi, J. M.; Miyazaki, M.; Stoehr, J. P.; Lan, H.; Kendziorski, C .M.; Yandell, B. S.; Song, Y.; Cohen, P.; Friedman, J. M.; Attie, A. D. Loss of stearoyl-CoA deasturase-1 function protects mice against adiposity. *Proc. Natl. Acad. Sci. U.S.A.* **2002**, *99*, 11482–11486.

(3) Miyazaki, M.; Kim, Y.-C.; Gray-Keller, M. P.; Attie, A. D.; Ntambi, J. M. Stearoyl-CoA desaturase-1 mediates the pro-lipogenic effects of dietary saturated fat. *J. Biol. Chem.* **2000**, *275*, 30132–30138.

(4) Miyazaki, M.; Flowers, M. T.; Sampath, H.; Chu, K.; Otzelberger, C.; Liu, X.; Ntambi, J. M. Hepatic stearoyl-CoA desaturase-1 deficiency protects mice from carbohydrate-induced adiposity and hepatic steatosis. *Cell Metab.* **2007**, *6*, 484–496.

(5) Jiang, G.; Li, Z.; Liu, F.; Ellsworth, K.; Dallas-Yang, Q.; Wu, M.; Ronan, J.; Esau, C.; Murphy, C.; Szalkowski, D.; Bergeron, R.; Doebber, T.; Zhang, B. B. Prevention of obesity in mice by antisense oligonucleotide inhibitors of stearoyl-CoA desaturase-1. *J. Clin. Invest.* **2005**, *115*, 1030–1038.

(6) Gutierrez-Juarez, R.; Pocai, A.; Mulas, C.; Ono, H.; Bhanot, S.; Monia, B. P.; Rossetti, L. Critical role of stearoyl-CoA desaturase-1 (SCD1) in the onset of diet-induced hepatic insulin resistance. *J. Clin. Invest.* **2006**, *116*, 1686–1695.

(7) Xu, H.; Wilcox, D.; Nguyen, P.; Voorbach, M.; Smith, H.; Brodjian, S.; Suhar, T.; Reilly, R. M.; Jacobson, P. B.; Collins, C. A.; Landschulz, K.; Surowy, T. K. Hepatic knockdown of stearoyl-CoA desaturase 1 via RNA interference in obese mice decreases lipid content and changes to fatty acid composition. *Front. Biosci.* **2007**, *12*, 3781–3794.

(8) Li, C. S.; Belair, L.; Guay, J.; Murgasova, R.; Sturkenboom, W.; Ramtohul, Y. K.; Zhang, L.; Huang, Z. Thiazole analog as stearoyl-CoA desaturase 1 inhibitor. *Bioorg. Med. Chem. Lett.* **2009**, *19*, 5214–5217.

(9) Leger, S.; Black, W. C.; Deschenes, D.; Dolman, S.; Falgueyret, J. P.; Gagnon, M.; Guiral, S.; Huang, Z.; Guay, J.; Leblanc, Y.; Li, C. S.; Masse, F.; Oballa, R.; Zhang, L. Synthesis and biological activity of a potent and orally bioavailable SCD inhibitor (MF-438). *Bioorg. Med. Chem. Lett.* **2010**, *20*, 499–502.

(10) Ramtohul, Y. K.; Black, C.; Chan, C.-C.; Crane, S.; Guay, J.; Guiral, S.; Huang, Z.; Oballa, R.; Xu, L.-J.; Zhang, L.; Li, C. S. SAR and optimization of thiazole analogs as potent stearoyl-CoA desaturase inhibitors. *Bioorg. Med. Chem. Lett.* **2010**, *20*, 1593–1597.

(11) Issandou, M.; Bouillot, A.; Brusq, J.-M.; Forest, M.-C.; Grillot, D.; Guillard, R.; Martin, S.; Michiels, C.; Sulpice, T.; Daugan, A. Pharmacological inhibition of stearoyl-CoA desaturase 1 improves insulin sensitivity in insulin-resistant rat models. *Eur. J. Pharmacol.* **2009**, *618*, 28–36.

(12) Koltun, D. O.; Zilbershtein, T. M.; Migulin, V. A.; Vasilevich, N. I.; Parkhill, E. Q.; Glushkov, A. I.; McGregor, M. J.; Brunn, S. A.; Chu, N.; Hao, J.; Mollova, N.; Leung, K.; Chisholm, J. W.; Zablocki, J. Potent, orally bioavailable, liver-selective stearoyl-CoA desaturase (SCD) inhibitors. *Bioorg. Med. Chem. Lett.* **2009**, *19*, 4070–4074.

(13) Attie, A. D.; Krauss, R. M.; Gray-Keller, M. P.; Brownlie, A.; Miyazaki, M.; Kastelein, J. J.; Lusis, A. J.; Stalenhoef, A. F. H.; Stoehr, J. P.; Hayden, M. R.; Ntambi, J. M. Relationship between stearoyl-CoA desaturase activity and plasma triglycerides in human and mouse hypertriglyceridemia. *J. Lipid Res.* **2002**, *43*, 1899–1907.

(14) Hulver, M. W.; Berggren, J. R.; Carper, M. J.; Miyazaki, M.; Ntambi, J. M.; Hoffman, E. P.; Thyfault, J. P.; Stevens, R.; Dohm, G. L.; Houmard, J. A.; Muoio, D. M. Elevated stearoyl-CoA desaturase-1 expression in skeletal muscle contributes to abnormal fatty acid partitioning in obese humans. *Cell Metab.* **2005**, *2*, 251–261.

(15) Miyazaki, M.; Man, W. C.; Ntambi, J. M. Targeted disruption of stearoyl-CoA desaturase1 gene in mice causes atrophy of sebaceous and meibomian glands and depletion of wax esters in the eyelid. *J. Nutr.* **2001**, *131*, 2260–2268.

(16) Kasuya, T.; Kuroda, S. Nanoparticles for human liver-specific drug and gene delivery systems: in vitro and in vivo advances. *Expert Opin. Drug Delivery* **2009**, *6*, 39–52.

(17) Erion, M. D.; Bullough, D. A.; Lin, C.-C.; Hong, Z. HepDirect prodrugs for targeting nucleotide-based antiviral drugs to the liver. *Curr. Opin. Invest. Drugs* **2006**, *7*, 109–117.

(18) Smith, N. F.; Figg, W. D.; Sparreboom, A. Role of the liver-specific transporters OATP1B1 and OATP1B3 in governing drug elimination. *Expert Opin. Drug Metab. Toxicol.* **2005**, *1*, 429–445.

(19) Girardin, M.; Alsabeh, P. G.; Lauzon, S.; Dolman, S. J.; Ouellet, S. G.; Hughes, G. The regiochemistry of the ester group in **17** was confirmed by an independent synthetic route involving the coupling of the amine component with a bromoisoxazoline intermediate. *Org. Lett.* **2009**, *11*, 1159–1162.

(20) Joshi, V. C.; Wilson, A. C.; Wakil, S. J. Assay for the terminal enzyme of the stearoyl coenzyme A desaturase system using chick embryo liver microsomes. *J. Lipid Res.* **1977**, *18*, 32–36.

(21) Zhang, L.; Ramtohul, Y.; Gagné, S.; Styler, A.; Wang, H.; Guay, J.; Huang, Z. A multiplexed cell assay in HepG2 cells for the identification of delta-5, delta-6, and delta-9 desaturase and elongase inhibitors. *J. Biomol. Screening* **2010**, *15*, 169–176.

(22) Liu, G.; Lynch, J. K.; Freeman, J.; Liu, B.; Xin, Z.; Zhao, H.; Serby, M. D.; Kym, P. R.; Suhar, T. S.; Smith, H. T.; Cao, N.; Yang, R.; Janis, R. S.; Krauser, J. A.; Cepa, S. P.; Beno, D. W. A.; Sham, H. L.; Collins, C. A.; Surowy, T. K.; Camp, H. S. Discovery of potent, selective, orally bioavailable stearoyl-CoA destaurase 1 inhibitors. *J. Med. Chem.* **2007**, *50*, 3086–3100.

(23) hSCD1 assay: Powell, D.; Lebrun, M.-E.; Bhat, S.; Ramtohul, Y. K. Patent WO2009/129625, 2009.

(24) Volpe, D. A. Drug permeability studies in regulatory biowaiver applications. *Drug Absorption Stud. Biotechnol.: Pharm. Aspects* **2008**, *5*, 665–680.

(25) Kirby, B. J.; Unadkat, J. D. Grapefruit juice, a glass full of drug interactions? *Clin. Pharmacol. Ther.* **2007**, *81*, 631–633.

(26) Other OATP substrates such as statins have been shown to have intestinal absorption by OATPs: Shirasaka, Y.; Suzuki, K.; Nakanishi, T.; Tamai, I. Intestinal absorption of HMG-CoA reductase inhibitor pravastatin mediated by organic anion transporting polypeptide. *Pharm. Res.* **2010**, *27*, 2141–2149.

(27) Bleasby, K.; Castle, J. C.; Roberts, C. J.; Cheng, C.; Bailey, W. J.; Sina, J. F.; Kulkarni, A. V.; Hafey, M. J.; Evers, R.; Johnson, J. M.; Ulrich, R. G.; Slatter, J. G. Expression profiles of 50 xenobiotic transporter genes in humans and pre-clinical species: a resource for investigations into drug disposition. *Xenobiotica* **2006**, *36*, 963–988.

(28) Konig, J.; Cui, Y.; Nies, A. T.; Keppler, D. A novel human organic anion transporting polypeptide localized to the basolateral hepatocyte membrane. *Am. J. Physiol. Gastrointest. Liver Physiol.* **2000**, *278*, G156–164.

(29) Lan, R.; Liu, Q.; Fan, P.; Fernando, S. R.; McCallion, D.; Pertwee, R.; Makriyannis, A. Structure−activity relationships of pyrazole derivatives as cannabinoid receptor antagonists. *J. Med. Chem.* **1999**, *42*, 769–776.

(30) Talber, R. L. Safety issues with statin therapy. *J. Am. Pharm. Assoc.* **2003**, *46*, 479–488.

(31) Niemi, M. Role of OATP transporters in the disposition of drugs. *Pharmacogenomics* **2007**, *8*, 787–802.

(32) SEARCH Collaborative Group.. *SLCO1B1* Variants and statin-induced myopathy—a genomewide study. *N. Engl. J. Med.* **2008**, *359*, 789–799.